Evaluation of potential flow models for unsteady separated flow with respect to experimental data

Field Manar and Anya R. Jones

An evaluation of potential flow models for unsteady separated flow with respect to experimental data

Field Manar[*] and Anya R. Jones[†]

University of Maryland, College Park

(Dated: February 15, 2019)

The wake characteristics and force production of an aspect ratio eight flat plate rectangular wing starting from rest at high angle of attack ($\alpha = 45°$) were examined. The first portion of this paper presents experimental measurements that focus on circulation production at the leading edge of the wing. Circulation production is shown to be coupled to both the wing kinematics and the wake state. The second portion of the paper reviews the implementation of several pertinent potential flow models from the literature, and compares the results of these models to the experimental results. Quasi-steady and fixed wake models were found to be poor predictors of both force and circulation. A similarity solution based model was found to make accurate predictions only at very short times. An unsteady strength two-vortex model predicted the circulation production during the acceleration portion of the kinematics, but did not predict the force. A multiple discrete vortex model was found to predict both the force and circulation production well, but had difficulty after the shedding of the first leading-edge vortex.

I. INTRODUCTION AND BACKGROUND

Unsteady aerodynamics has been studied since the early days of the aerospace field, spurred largely by the aeroelastic problems encountered in fixed wing flight. As a result, the theories of attached unsteady flow are well developed and understood, for example, a comprehensive overview can be found in Bisplinghoff, Ashley, and Halfman [1]. The same cannot be said of unsteady flows with leading-edge separation, which are still an open research topic [2]. The original impetus for the current work stemmed from interest in reproducing insect-like flapping wing flight in small unmanned "micro air vehicles" (MAVs). The realization of this dream has not yet come to pass in a meaningful way, due in part to limited aerodynamic understanding and a lack of applicable models of the unsteady separated flows that such vehicles rely on.

Study of flapping wing aerodynamics has revealed that, in general, the flows encountered in flapping wing flight are similar to stalled transient flows. Furthermore, small fliers of any type must overcome the difficulties inherent to the low Reynolds number flight regime [3] and MAV applications naturally require operation in a Reynolds number range of $Re = \mathcal{O}(10^2 - 10^5)$, much lower than traditional aerospace applications. This reduction in Reynolds number leads to poor performance of traditional thick airfoils [4, 5]. The combined effect of low Reynolds numbers and the likelihood of encountering large angles of attack makes separation and dynamic stall nearly a foregone conclusion for MAV flight. Efforts to model leading-edge separated flows are thus applicable to a broad range of problems and can be applied to insect flight, MAV gust encounters, dynamic stall, and wind and tidal turbine flows.

In order to study the phenomena of leading-edge separation from a first-principles approach, the problem has been systematically reduced. The first reduction is to use a rectangular flat plate wing as a representative geometry. The wing used here, and in many other studies, is a thin flat plate with square edges; this is not too far removed from an insect wing and serves as a canonical geometry for experimentation.

The second reduction is to distill the flapping wing kinematics from oscillatory three degree-of-freedom flapping about a shoulder joint to a rectilinear surge at constant angle of attack. These simpler kinematics are closest to the start and mid-stroke portions of the full insect kinematics, but still differ in their disregard of the rotational component of motion. Both of these simplifications are common to the field.

As a surrogate for the complete insect wing kinematics, many studies have instead used translating wing motions to study the problem at hand (e.g. Dickinson and Gotz [6]). This is generally done to produce simpler, easier to understand flows. As such, rectilinear pitching and surging kinematics have been particularly well documented in both experimental [7–9] and computational studies [10–13]. Rotating wings, i.e. a wing revolving about its root, are another common surrogate for the insect wingstroke [14–19]. These preserve the rotation of the entomological flapping wing in the stroke plane, but neglect the out-of-plane motion. In general, studies on simplified wing kinematics have produced a large body of data that serves as a quantitative reference for the cases considered here [2], but

[*] fmanar@umd.edu
[†] arjones@umd.edu

the need for a computationally inexpensive predictive model remains.

Traditionally, those who seek to model unsteady separated flows and predict the forces from first principles have used only the flow visualization and force measurements from experimental studies (e.g. Hammer *et al.* [20], or Wang and Eldredge [21]). However, for a model of even modest complexity, the force results are an amalgamation of all parts of the model interacting, and using the force histories in an attempt to diagnose the success of a model leads to vague answers at best. This state of affairs has led to the continued use of the leading-edge Kutta condition while simultaneously doubting its validity. The caveat is usually then given that the Kutta condition is inappropriate for the leading edge because flow separates here in the wing-normal direction rather than tangential to the leading edge. In the current work, the form of Kutta condition used is to enforce flow (and therefore the forming vortex sheet) tangent to the plate. The separation point is also assumed to be fixed at the leading edge. Further discussion of the Kutta condition is reserved for section II C.

The leading-edge vortex (LEV) is a prominent feature in both dynamic stall events [22] and insect flight [23]. It forms when the wing motion is aggressive enough to cause the flow to separate from the leading edge of the wing and roll up into a vortex above the suction side of the wing [2]. The flow field is dominated by this vortex, which in turn dominates the force production of the wing [6, 24]. The LEV forms because the sharp leading edge forces the boundary layer to separate there, which then rolls up into a single vortex. Several models of LEV growth have been developed based on the leading edge conditions [25–30]. Most of these studies are concerned with an oscillating wing (e.g. Buchholz *et al.* [26] and Widmann and Tropea [30]), so the scaling laws they present are largely based on the parameters of the oscillation. This produces valuable insights, but can obfuscate the underlying mechanisms for the circulation growth. For example, including the amplitude as a scaling factor, as in Buchholz *et al.* [26], does not make it clear if the vortex is larger because of the increased wing speed or because of the greater distance covered during the wing motion.

On the other hand, Sattari *et al.* [27] proposed using the boundary layer exterior velocity to capture the flux of vorticity in a feeding shear layer from the trailing edge of a waving plate. Kriegseis *et al.* [28] built on this idea and used the total flow velocity at the leading edge to successfully collapse the LEV circulations of wings plunging with different plunge amplitude. In their paper, the total flow velocity just outside the shear layer is used as a surrogate for the

strength of the feeding shear layer. Wong *et al.* [29] and Widmann *et al.* [30] use a similar philosophy to estimate the size of the LEV.

Vorticity flux measurements similar to those conducted here have been carried out by Panah *et al.* [31] and Wojcik and Buchholz [25]. These studies were primarily concerned with establishing the importance of the secondary vorticity produced in the opposite-sign boundary layer below the LEV. The analysis of Lighthill [32] indicated that the surface pressure gradient is directly related to the vorticity production at a fluid/solid interface. To measure the secondary vorticity production, Panah *et al.*'s study included surface pressure measurements. Based on these pressure measurements, both Panah *et al.* [31] and Wojcik and Buchholz [25] concluded that the opposite-sign vorticity production on the surface of the plate contributed approximately half the magnitude of circulation as the shear layer from the leading edge to the circulation of the leading-edge vortex. Both of these studies, however, focused on kinematics dissimilar to the present surge case: Panah *et al.* [31] used an oscillating plunging wing, and Wojcik and Buchholz [25] used a rotating wing. In both of these cases the LEV is held nearer to the wing than is seen in pure translation, likely resulting in a stronger secondary boundary layer below the LEV.

To remedy these gaps in the literature, the current work focuses on a series of experiments conducted to directly measure circulation production at the leading edge of a wing starting from rest. Current low-order physics-based modeling techniques are then evaluated in the context of these measurements. The goal of the model evaluation presented here is to assess the strengths and weaknesses of the current methods and identify avenues for improvement. Close inspection of these models also aids in understanding how the forces produced relate to the fluid processes.

II. POTENTIAL FLOW MODELING

Interest in flapping wing flight and unsteady aerodynamics in general has produced a plethora of approaches to predicting the forces on a wing undergoing unsteady motion. The extant models run the gamut from rigorous analytical analysis [33–37], to modified versions of classical theories [38, 39], to vortex-based computational schemes [21, 40–44], empirically based models [45–47], grid-based CFD methods [48–50], and viscous vortex particle methods [10].

The motivation behind the choice of models presently being examined is to focus on those models suitable for engineering work, i.e. to trade accuracy

for quick computation, while still including the requisite physics. Which physics are required is still something of an open question; at a minimum the models should be able to predict the presence and bulk characteristics of the LEV. Ideally, the model would also include a prediction of the shedding process. Preference is given to techniques that neatly categorize the various contributors to the force, as this aids in developing intuition. These requirements point the researcher towards potential flow theory. Potential flow has long been the bastion of pen and paper solutions, and also gave rise to the more versatile panel methods still in use today. Potential flow, and thus panel methods, rely on a few key simplifications, namely inviscid and incompressible flow. These assumptions are largely appropriate for the present class of problems, but it should be noted that applying these models at the Reynolds numbers considered here ($\mathcal{O}(10^4)$) stretches the limits of the inviscid assumption. Nevertheless, the formation of the LEV from the shear layer presents itself as a convection-dominated process, rather than diffusive one.

Any unsteady potential flow model consists of three components: a representation of the body, a representation of the wake, and a method for determining the circulation. For a general introduction to potential flow theory, the reader is referred to any number of fluids texts [51–55], but an overview is appropriate here to understand where the models used in the present work come from.

A. Body Representation

The first consideration when modeling an external flow problem is how to represent the body in question. The body comes into the equations as a no-penetration boundary condition for the fluid at the body surface. Stated simply, it says that the fluid velocity at the body surface must match that of the body in their surface-normal components. To enforce this, several methods have been developed throughout history: conformal mapping, basis functions for a vortex sheet, and panel methods. These methods all converge on the same solution, and are largely interchangeable outside of the details of their implementation.

The oldest method for meeting the no through-flow boundary condition is to use conformal mapping. It is the foundation for the basic unsteady flow solutions that are known throughout the aerospace field such as Wagner's problem of an impulsively started plate [33], or Theodorsen's frequency response [35]. Despite its age, the conformal mapping method still enjoys popularity in recent work on un-

steady separated flows, and is the basis for methods such as Wang and Eldredge [21], Xia and Mohseni [56], Ansari *et al.* [41, 57], and Minotti [58]. Conformal mapping methods imply the use of a complex potential formulation. The method works by stretching space so that a flat plate is mapped to a cylinder. Arbitrary body shapes can be accommodated by extending the series of the mapping or by using the Schwartz-Christoffel transform.

The no-penetration boundary condition can also be also be fulfilled by solving for the strength of the surface vortex sheet. When the body is infinitely thin, a common approach is to parameterize the strength of that sheet with a truncated series expansion. One must then solve for the coefficients of the series expansion to enforce the no through-flow condition at a finite number of collocation points. The two most common basis for the series are a modified Fourier series (usually attributed to Glauert [59]), and a Chebyshev series [40, 43, 60]. In either case, the body is typically represented by a vortex sheet, although it is also possible to use a doublet sheet.

The strength of basis function methods lies in their ability to capture either the singularities at the ends of the plate or naturally enforce the Kutta condition, while still maintaining a tradeoff between numerical and analytical computation. They also provide a sound analytical basis for the edge suction parameter, which relies on properly capturing the square-root singularity in sheet strength at the edge. The primary drawback of using basis functions is that they do not extend to arbitrary geometry (e.g. thick airfoil profiles) without explicit modification on the part of the user. It is still less clear how to apply them for 3D problems.

An alternative method to solve for the vortex sheet strength is to use a series of discrete panels, in much the same way as a finite element method. Instead of representing the singularity strength with a few complicated functions that span the domain, it is now represented with many simple functions with limited support. Originally developed for non-lifting flows by Hess and Smith [61, 62], panel codes have developed into a practical and general design tool for both 2D and 3D flows. A good overview of panel methods is given in Katz and Plotkin [52]. While extremely flexible, it is difficult to capture the singularities that naturally occur at the edges of bound vortex sheets with this method.

B. Wake Representation

In addition to computing the effect of the body, potential models for unsteady flow require the inclusion of vorticity in the fluid. The job of the wake

representation is to provide a discrete representation of that vorticity and to propagate the wake forward in time by solving the vorticity evolution equation. In two dimensions with the inviscid and incompressible assumptions, vorticity evolution is simply a statement that fluid particles that have vorticity keep that vorticity, and so any vorticity must therefore convect with the fluid. Convecting the vorticity with the fluid leads naturally to a Lagrangian formulation, where propagating the wake in time boils down to convecting the discrete representation with the flow. (To fully solve the vorticity form of Navier-Stokes also requires accounting for diffusion and, in three dimensions, vortex stretching.) An Eulerian approach is also possible, but these methods require meshing the full fluid volume and are not as generalizable to low order models. They will not be considered here.

The most convenient way to discretely represent the vorticity field in potential models is to add point vortices that convect with the fluid. This leads to the class of methods known as vortex methods, discussed in detail in Cottet and Koumoutsakos [63] and Saffman [64]. A problem with pure point vortices is that their induced velocity tends to infinity the closer one gets to them. This causes difficulties in numerical simulations, where particles that are in too close proximity can garner unrealistically high induced velocities and convect themselves out of the simulation domain. The same high velocities also help propagate instabilities in vortex sheets, causing the interior structure of rolled-up sheets (as in the LEV) to fall apart and become chaotic. To counter this, the vortex can be regularized with a vortex core model that spreads the vorticity over a finite area rather than a point. The first such methods were proposed by Chorin, Krasny, and Bernard to study the problem of vortex sheet roll-up [65–67]. They used a non-physical model of the vortex core that simply added a constant factor to the distance between the vortex and the interrogation point. Other models, such as the more physical Rankine, Burgers, or Lamb-Oseen vortex core can also be used, but are often overlooked because of their computational cost. An approximation of the Lamb-Oseen vortex core is proposed by Vatistas *et al.* [68], and has been used for computations such as those by Ramesh *et al.* [44].

The concept of a point vortex is applicable in both two and three dimensions, but the vorticity evolution equation has additional terms in three dimensions. Extra work is required to compute vortex stretching and keep the resulting vorticity field divergence free. That extra work is made easier when information about the arrangement of the point vortices is kept. This leads to the implementation of higher order discretizations of the vorticity. In two dimensions, besides point vortices (a zero-dimensional representation) it is possible to have vortex lines [40, 43] and patches. Constant strength vortex patch methods are referred to as contour dynamics methods [69]. In three dimensions, line vortices are by far the most common element, and lead to the vortex lattice methods (see, once again, Katz and Plotkin [52]). It is also possible to have sheets [70, 71], or volumes. These are attractive, but adding this extra dimensionality also adds to the computational cost, and often requires ad hoc methods to manage the connection between particles when things become tangled. An excellent, if somewhat informal, review of vortex methods is given by Stock [72].

C. Circulation Conditions

There are three prevailing philosophies for dealing with the creation of vorticity in potential methods. One is to match the full no-slip surface condition and to fully resolve the boundary layer. Methods using this approach account for separation by capturing the boundary layer dynamics. Examples of this class of methods can be found in Winckelmans and Leonard's overview of early work in the field [73], Eldredge's VVPM method [10], the VRM method [74], or Kirchart and Obi's recent work [75]. Resolving the boundary layer requires large numbers of particles, however, and it is not uncommon to see particle counts in the hundreds of thousands to millions of particles. With such a large particle count comes a commensurate increase in computation time, making these methods undesirable for the present goal of low-cost computations. A second option is to use the integral boundary layer formulation coupled with the potential solver, as presented by Drela [76]. Unfortunately, outside of some preliminary work, these methods are limited to steady attached flows, and are of little use here. The third philosophy is to allow for a slip velocity on the body surface, thus representing the boundary layer as an infinitely thin vortex sheet. When surface slip velocity is allowed, potential flow provides no mechanism with which to generate circulation, and is mathematically non-unique with regard to total circulation. A surrogate circulation condition, such as the Kutta condition, must be applied at the separation point and in the case of unsteady flows, additional vortices are added at the separation point to maintain both the total circulation and the specified edge condition. This approach keeps particle counts, and therefore the computational cost, much lower than when resolving the full boundary layer. Note that

the separation point must be specified from prior knowledge, or solved for with an additional layer of modeling. Fortuitously, the separation point in attached flows is always the trailing edge and the shedding of vorticity is well described by the Kutta condition.

The de-facto standard for specifying circulation in potential flow models is the Kutta condition. There are many ways to express the condition and a bewildering number of ways to implement it. As Sarpkaya [77] puts it in his vortex method overview: "almost every paper, at least in part, represents a new method." The most common implementation is to enforce that the flow leave tangent to the shedding edge by adding a new wake vortex at each time step. At a minimum, this leaves the selection of the new vortex's location as an open question. In practice though, most methods achieve the same end result albeit perhaps through a different implementation. (A direct comparison of the various implementations, while tedious to construct, could be very enlightening.)

For the steady case, the Kutta condition is commonly implemented by enforcing zero bound vortex sheet strength at the edge of the plate, i.e.

$$\gamma(\tilde{x} = \tilde{x}_{TE}) = 0, \tag{1}$$

where γ is the vortex sheet strength in circulation per distance, and $\tilde{x}_{TE}$ is the location of the trailing edge in the plate frame of reference. When conformal mapping is used, the infinitely thin plate is mapped to a cylinder. The complex plane with the cylinder has locations notated with ζ, and the cylinder is centered at the origin with radius one. The expression of the Kutta condition specifies that the complex velocity, $W = u - iv$, at the edges of the plate in the ζ-plane are zero, i.e.

$$W(\zeta = \pm 1) = 0. \tag{2}$$

This has the effect of canceling the singular factor in the mapping from the cylinder back to the plate plane, resulting in a finite edge velocity and streamlines leaving smoothly from the edge. For the steady translation case, the only velocity components present are the translation and bound vortex components. This leads to a simple expression for the bound vortex strength,

$$\Gamma = -\pi c \tilde{V}, \tag{3}$$

where Γ is the circulation of the bound vortex, c is the chord, and $\tilde{V}$ is the plate-normal component of velocity at the midchord. When substituted back into the expressions for force and moment, the usual results of a two-dimensional lift coefficient

$C_l = 2L/\rho U^2 c = 2\pi \sin(\alpha)$ (for a freestream velocity U and angle of attack, α) and zero moment at the quarter chord are obtained. For the unsteady case, the concept of fixing the ζ-plane velocity at the plate edges to zero at all times remains. This method is implemented reactively, in the sense that the simulation is updated with new circulation to remove the erroneous edge velocity at each time step. Thus it does not lend itself to an analytical expression of the circulation rate, $d\Gamma/dt$.

Without resorting to conformal mapping, i.e. when using basis functions or a panel method, the correct form of the condition, according to the work of Krasny [78, 79] and Jones [40], is to put the ultimate focus on removing any infinite velocities in the flow. Doing this enforces that the pressure at the edge of the plate remains finite, and that the flow leaves tangential to the edge, two criteria often given as the Kutta condition. This leads to the extremely simple result that

$$\frac{d\Gamma}{dt} = \gamma u \tag{4}$$

where $d\Gamma/dt$ is the rate of circulation being added to the shed vortex sheet, γ is the bound vortex sheet strength at the edge of the plate, and u is the tangent velocity at the plate edge. This, like the conformal mapping method, is difficult to use as the basis for an analytical expression of circulation production. The first issue is that γ ties together everything in the flow field, including the motion of the plate and the location and strength of all wake vorticity. Further, the true value of γ is generally unbounded at the plate edge unless the Kutta condition is already precisely met. Hence most implementations, as mentioned previously, enforce the Kutta condition reactively.

Part of the reason that a plethora of methods exist for implementing the Kutta condition is that it is not clear from the statement of the Kutta condition alone how exactly to add the new circulation required to maintain the specified edge condition. In a point vortex model, the question becomes where to place the new vortices. A popular answer given by Ansari et al. [41] is to place the new vortex one-third of the distance from the edge to the most recently shed vortex. For finite-angle trailing edges (i.e. on thick airfoil shapes) Xia and Mohseni [80] recently proposed a rigorous momentum analysis to theoretically compute the angle and strength of a newly created vortex sheet that was found to improve solutions for rapid airfoil pitching.

In the present problem, separation is fixed at the leading and trailing edges of the flat plate wing. Unlike the trailing edge, it is not clear a priori that the Kutta condition is valid or useful at the leading

edge. A general statement of the Kutta condition is that the flow must leave tangent to the separating edge. Based on flow visualization, the separated leading-edge shear layer appears to leave in an approximately plate-normal direction. This difference of direction calls the validity of the Kutta condition into question. Nonetheless, it is a common choice.

The leading edge suction parameter (LESP), as proposed by Ramesh *et al.* [44], is a relaxation of the Kutta condition to allow for the presumed ability of finite thickness wing profiles to support a suction force at the leading edge [42]. This idea has been seen elsewhere, as in the philosophy behind the vortex shedding portion of Leishman-Beddoes model [81] and Polhamus's suction analogy [38]. In their paper, Ramesh *et al.* argue that for a given geometry and Reynolds number, the LESP provides a description of whether the leading-edge flow is attached or separated that is independent of wing kinematics. The LESP also has the enviable property of reducing to the Kutta condition when the allowable suction is set to zero.

Having now identified the key components and challenges of modeling separated flows using inviscid models, some experimental results are presented in the next section to provide an overview of the evolution of the real flow field. Following this, in Section IV, these results are compared to those of the models described above to identify the strengths and weaknesses of the various approaches and so identify the dominant physical phenomena in these types of flows.

III. EXPERIMENTAL RESULTS

This section presents detailed results for a single test case of an aspect ratio eight, $76.2\,\mathrm{mm}$ chord, flat plate wing in rectilinear translation at a constant angle of attack of $45°$. The width of the towing tank was $1.5\,\mathrm{m}$, approximately 2.5 times the span of the wing. The plate velocity was piecewise linear in time, a constant acceleration over two chord-lengths of travel followed by a transition to a constant final velocity, U_f, such that $Re = 12,500$. The velocity profile was slightly smoothed at the start and end of the acceleration to reduce vibrations. Because the wing mounting structure limited optical access at the center of the wing, flowfield measurements were acquired one chord-length off of the centerline. This location on the aspect ratio eight wing was shown by comparison to other spanwise locations and on shorter aspect ratio wings to have a nearly two-dimensional flow. Results from this motion are averaged over 5 runs and plotted with respect to non-dimensional time, $t^* = tU_f/c$. This case is rep-

resentative of the common features in wing start-up transients at high incidence. By studying this case in depth, the reader will be familiarized with the general picture of the real flow so that later comparisons to model predictions will be put in context. The experimental methods employed are documented in the appendix.

A. Flow Visualization

The vorticity fields for the baseline case described above were found via particle image velocimetry (PIV) measurements and are shown in fig. 1. Artifacts of the laser shadow are visible in the images as the light red diagonal lines under the wing, but in general, using vorticity as a flow visualization tool highlights the locations of shear and rotation in the flow, e.g. the boundary layers, shear layers, and vortices. As can be seen in the first image (top left, $t^* = 1$), the vorticity in the flow is initially confined to boundary layers very close to the wing surface. At the edges of the wing, the leading-edge (LEV) and trailing-edge (TEV) vortices have already begun to develop. As time progresses ($t^* = 2, 3, 4, 5$), flow leaves smoothly from the trailing edge of the wing, forming a starting vortex made up of a series of small-scale vortices centered at the original location of the wing's trailing edge. Initially, the boundary layer at the leading edge of the wing is forced back onto the wing, but it quickly rolls up into an LEV (see $t^* = 2, 3$). As wing motion progresses, the LEV moves slightly off of the wing surface but remains in the vicinity of the body. While the LEV is near the wing, it continuously gathers circulation fed to it by a shear layer emanating from the leading edge.

Eventually, the LEV grows to a size where it can no longer be sheltered from the free stream behind the wing, and it begins to convect downstream ($t^* = 5, 6$). This is when even the two-dimensional picture of the flow starts to get complicated. A new TEV rolls up behind the wing at $t^* = 6$ and shortly thereafter another LEV forms as well ($t^* = 8, 9, 10$), followed by yet another TEV at $t^* = 12$. Under the right conditions (two dimensional, and Reynolds number dependent), this alternating shedding process continues and the wake becomes a Kármán vortex street. Indeed, the details of vortex formation after the initial LEV depend on almost every aspect of the flow and are extremely difficult to predict. In the present case, the wing is translating, has a finite aspect ratio, and a moderately high Reynolds number, so the flow devolves into a chaotic separated wake at longer times ($t^* > 30$) [51].

Because the LEV remains close to the wing during its formation, it is expected to have a large effect on
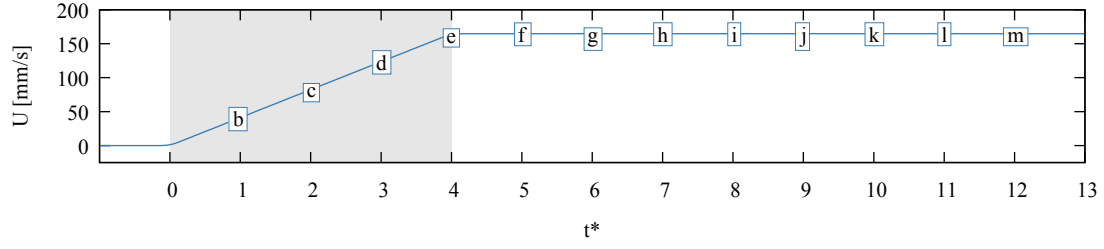
(a) Time history of wing velocity, indicating the timing of the flowfield images below.

(b) $t^* = 1$

(c) $t^* = 2$

(d) $t^* = 3$

(e) $t^* = 4$

(f) $t^* = 5$

(g) $t^* = 6$

(h) $t^* = 7$

(i) $t^* = 8$

(j) $t^* = 9$
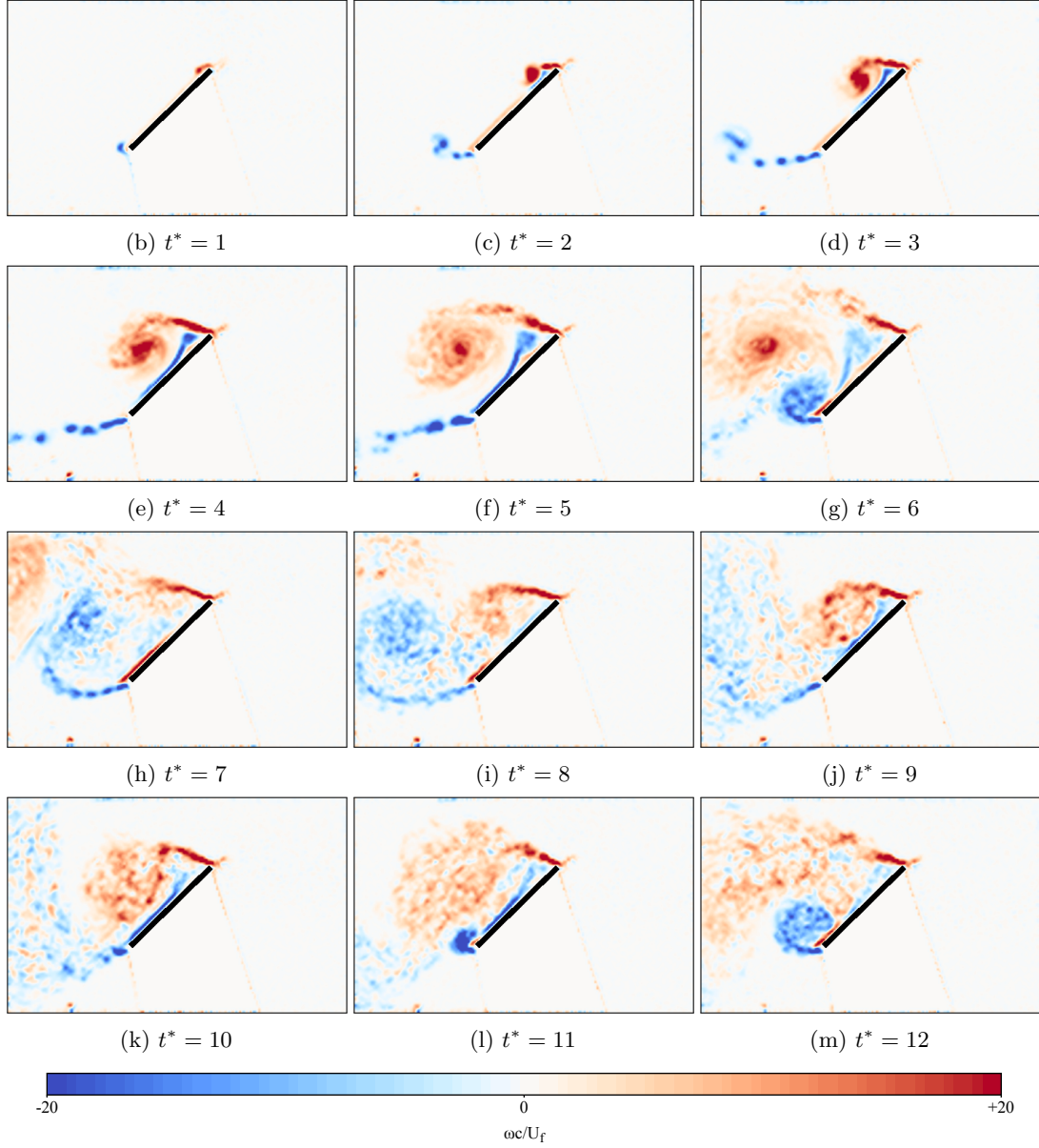
(k) $t^* = 10$

(l) $t^* = 11$

(m) $t^* = 12$

FIG. 1: Vorticity fields for a wing rapidly started in translation at 45° incidence, ensemble-averaged over 5 runs. The wing is moving from left to right, so the relative flow is from right to left. Red represents counterclockwise rotation; blue represents clockwise rotation.

the force and moment that the wing experiences; this will be borne out in the force data discussed in the next section. The development of the LEV has a direct effect on the fluid dynamic force on the wing even though the LEV is not fully attached to the wing, but eventually sheds. For this reason, the state and dynamics of the LEV are the primary focus of both measurements and modeling efforts.

B. Forces

It is intuitive that large changes in flow structure will correspond to an equally dynamic force history. The forces measured on the wing are shown in fig. 2 as a function of $t^* = tU_f/c$. The figure shows four different curves including the coefficients of lift, C_L, and drag, C_D, in the lab frame. The force coefficients in the wing-relative frame, the wing-normal, C_N, and the wing-tangential, C_T, coefficients are also shown. All of the force coefficients are defined with respect to the final wing velocity, U_f. Although there are some high-frequency small-scale oscillations in force visible in each of the curves due to the mechanical vibration of the towing carriage and wing mounting structure, the overall shape of the curves remains clear.

As shown in fig. 2, the lift and drag forces for the baseline case are essentially identical. This is a coincidence due to the choice of angle of attack, $\alpha = 45°$. A more universal observation for flat plates is that the majority of the force is concentrated in the wing-normal component while the tangential component is essentially zero. The lack of wing-tangential force in this case is a byproduct of the near complete flow separation. Neglecting viscous drag, the wing-tangential component of force is exactly the force associated with edge suction. Recall that the Kutta condition can be expressed as requiring zero suction at the edge of a wing. As in the attached-flow case, the Kutta condition is presumed to hold at the trailing edge so the lack of tangential force points to the enforcement of the Kutta condition at the leading edge of the wing as well.

Now focusing more on the shape of the curves, there are several distinct features. The forces on the flat plate wing start at zero in the quiescent flow, and motion begins at $t^* = 0$. At this time there is a rapid rise in force as the wing begins accelerating, with both the rise in force and wing's transition to full acceleration occurring over $t^* = 0.25$. This is followed by a continued rise to a distinct peak that slightly lags the end of the acceleration. Following that, forces slowly decay to steady state, though the decay is punctuated by several peaks. Based on the flow visualization given in fig. 1, one can attribute these local force maxima to the formation and shedding of LEVs above the wing. This process is particularly evident in the flowfield images at $t^* = 5$ and $t^* = 10$, which show large LEVs and correspond to the peaks in forcing visible in fig. 2. The cyclic shedding process observed through $t^* = 12$ gradually wears down, and the forces have nearly finished settling to a steady value by the time the wing has traveled about 30 chord-lengths ($t^* = 30$).

C. Vortex Tracking

Quantitatively measuring the wake behind the wing reveals further information about how the flow develops, and will turn out to be critical in the evaluation of potential flow models. The quantities shown here are all derived from PIV measurements of the LEV, as this is the dominant flow feature early in the motion of the wing. Quantification of the LEV helps to distinguish between cases that produce different forces on the wing but have visually similar LEV development.

Trajectories of the center of the LEV are shown in fig. 3. These figures contain tracks computed from both the vorticity centroid and Γ_1 criteria. (See Appendix for details.) Note that the Γ_1 data is restricted to the duration of time that the first LEV is in the imaging frame. The Γ_1 method tracks a rotation center and more closely aligns with the intuition of a vortex. Specifically, it tracks the initial coherent dominant leading-edge vortex. The vorticity centroid method has been extended to account for vorticity leaving the frame with a frozen wake hypothesis. The locations are normalized by the wing chord, and are relative to the leading edge. The centroid method does not make distinctions between separate vortices and shear layers, and includes all the vorticity shed from the leading edge. This provides a low order estimate for the net location of the wake vorticity rather than the specific location of a single coherent vortex.

Looking at the vortex convection in the wing frame, shown in fig. 3a, one sees the path of the vortex as it leaves the wing, as well as the discrepancy between the centroid and Γ_1 methods of vortex identification. Note that this figure does not indicate rate of convection, only location in space. Both methods indicate that the LEV leaves the suction surface of the wing from approximately a tenth of a chord behind the leading edge. The vortex center as identified using the centroid measurement method convects nearly straight aftwards, while that of the Γ_1 method convects slightly downwards. Results obtained using the centroid measurement also indicate a distinct hump in the height of the vortex between
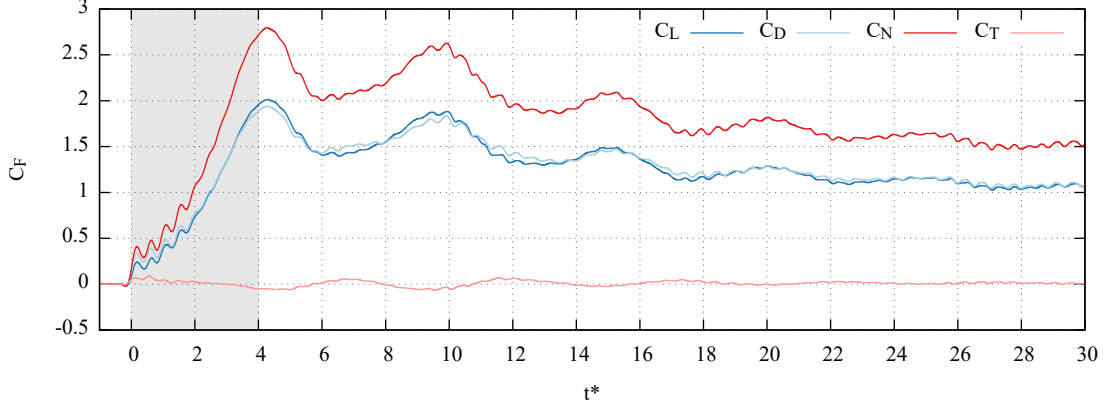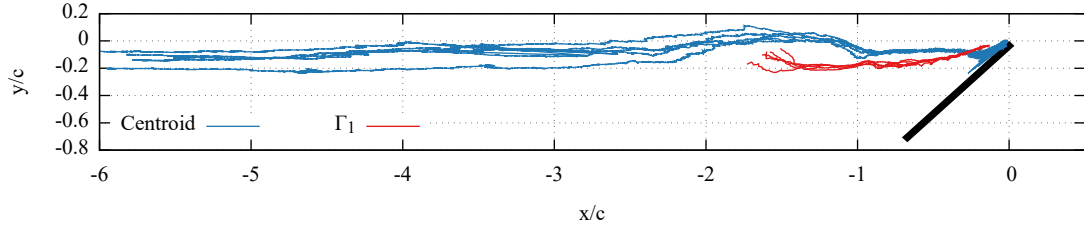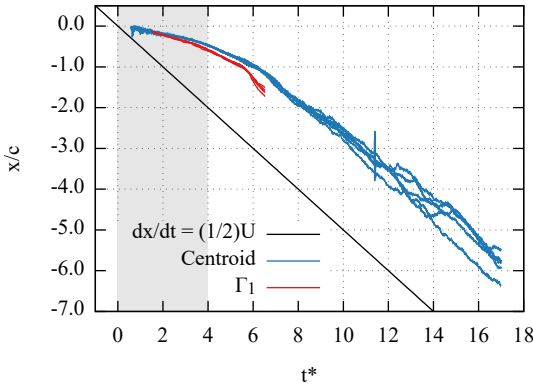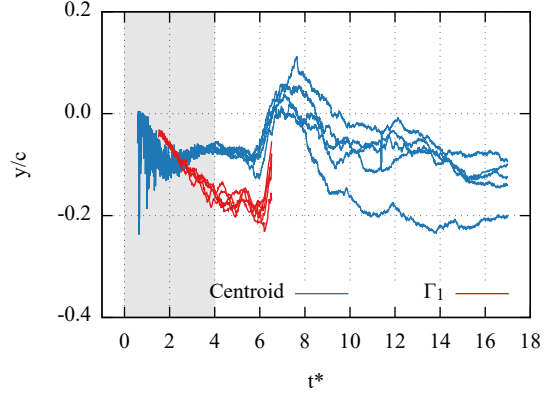
FIG. 2: The forces on an $AR = 8$ wing undergoing surge at $\alpha = 45°$. The shaded area corresponds to the acceleration portion of the velocity profile.

(a) Trajectory of the LEV in the wing frame.

(b) x-location of the LEV in time.

(c) y-location of the LEV in time.

FIG. 3: Vortex location measurements on a surging wing. Data from five independent trials is overlaid for both methods.

$x/c = -2$ and $x/c = -1$. Figure 3b indicates that the LEV is at $x/c = -1$ when $t^* = 6$. Referring back to fig. 1, note that the hump in the centroid-measurement results occurs at the same time that the trailing-edge vortex forms and pushes the initial LEV off the wing. It is interesting that this hump is not reflected in the Γ_1 measurements. This suggests that the center of rotation of the vortex is less af-

fected by TEV formation than is the overall vorticity field and leading-edge shear layer.

The plots given in figures 3b and 3c show the x- and y-locations of the LEV returned by both methods relative to wall clock time. Results from the centroid method have some noise at the beginning of the run when the LEV has not yet gathered enough strength to achieve a good signal-to-noise

ratio. During this time, the Γ_1 method is unable to conclusively identify an LEV. Figure 3b also includes a solid black line showing what the vortex location would be if it had convected downstream at a constant speed at half the freestream velocity. This would be the expected value if the circulation is produced at a constant rate, but the vortex initially convects slower than this. At early times ($t^* < 6$) the path of the LEV does not appear to be linear, but rather has a distinct curve indicative of the LEV convection velocity increasing in time. The increase in LEV convection picks up considerably at $t^* = 6$, which, as discussed previously, corresponds to the formation of the TEV and the shedding of the first LEV. Figure 3b shows that at long times ($t^* \geq 10$), the centroid of the LEV convects at close to half of the freestream velocity without any obvious deviations. This leads to the hypothesis that the circulation production at the leading edge of the wing reaches a relatively constant value, resulting in a roughly constant-vorticity wake.

The y-location, shown in fig. 3c, of the LEV is a bit more subtle in its development, staying nearer to zero (note smaller plot scale compared to x-location) for the duration of the wing motion and only falling slightly at late times. As a first-order approximation one could say that $y/c = 0$, especially up to $t^* = 6$. Higher order trends are difficult to generalize, though the Γ_1 method shows a downward trend that is not reported by the centroid method.

The first takeaway from the vortex tracking analysis presented here is that the leading-edge vortex is neither attached to the wing, nor is it swept away at the freestream velocity. From a modeling perspective, this means that the motion of the vortex cannot be accounted for with a simple assumption of fixed location either in the wing or in the lab reference frame, but instead requires knowledge of the vortex convection speed. Thus, to model the flow, an empirical rate of x-motion must be used, or the flow itself must by computed (e.g. with a potential flow model).

The second takeaway is that the exact trend in vortex location is difficult to determine from measurement. This stems from difficulty in precisely defining a vortex, especially in the present context of a growing vortex near a wing, and as such, it is not clear which tracking method will produce the "correct" vortex location. Furthermore, the first LEV can be tracked with reasonable success, but subsequent vortices are difficult to assess because of the turbulent nature of the flow. (Recall the flow images in fig. 1. That being said, the methods presented here do appear to be consistent, at least up to $t^* = 6$.

The vortex trajectories shown here will serve as one of the methods for evaluating models of unsteady flow. Vortex location and convection is a primary factor in determining the resulting force on the wing, and thus a quantification of model success in this regard helps point out some of the underlying causes for success and failure in predicting unsteady loading. The other vortex characteristic of primary concern is its strength, which will be discussed next.

D. Vortex Circulation

Because the amount of circulation produced at the leading edge of the plate directly feeds the leading-edge vortex and thereby affects the time history of the vortex strength, circulation production is one of the most critical components in determining the overall success of a flow model. The measured circulation flux, i.e., the time rate of vorticity passing through a boundary surrounding the leading edge, is shown in fig. 4 for the baseline case. The circulation flux is computed using a square box that measures $0.08c$ on each side and is centered at the leading edge of the wing. Circulation is computed by summing the product of vorticity and velocity normal to the box. Further implementation details of the measurement are documented in the appendix. The circulation flux as shown here relates directly to the rate of change of the total positive (i.e., counterclockwise) circulation in the flow field. Vorticity generated at the leading edge of the wing is always positive and is continuously produced, so the circulation flux through the boundary is also always positive, and thus the circulation of the leading-edge vortex monotonically increases. The overall shape of the circulation flux curve offers some interesting insights into what is required for modeling the flux, as well as the development of the leading-edge vortex and the overall flow field.

The circulation flux shown in fig. 4 increases nearly linearly from $t^* = 0.5$ as the wing accelerates, reaching a peak near $t^* = 3.5$. The peak occurs nearly in line with the end of acceleration, in contrast to measurement of the forces, which showed a peak after the end of acceleration (fig. 2). After this point, the wing moves at a constant velocity. The circulation flux, however, falls off and continues to change, passing through more peaks and valleys as it approaches a steady state. These maxima and minima correspond to the LEV formation and shedding process seen in the flow visualization. See fig. 1 at $t^* = 4$ for the first peak, $t^* = 6$ for the subsequent minimum, and $t^* = 9, 10$ for the second peak. These results share similarities with the work on vortex formation time, e.g. as reviewed by Dabiri [82]. Based on this case alone however, it is not clear that the
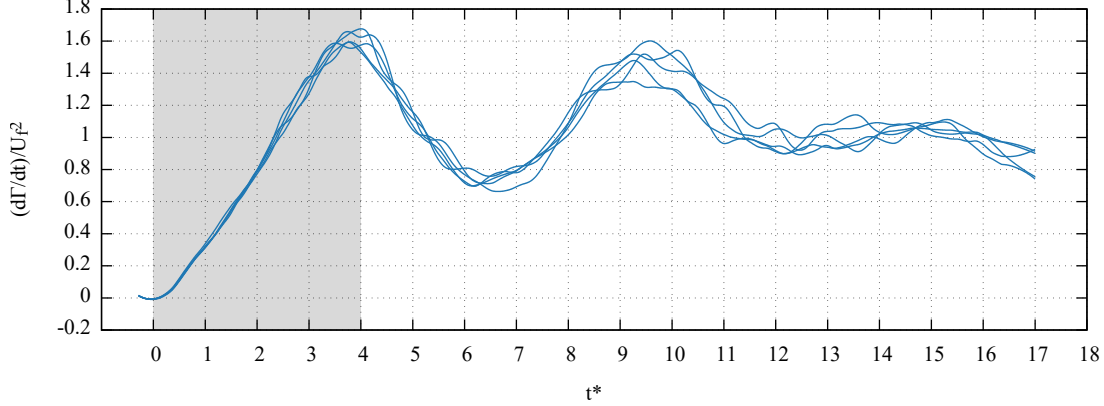
FIG. 4: Circulation production from the leading edge of the wing. The lines show filtered values from five separate trials.
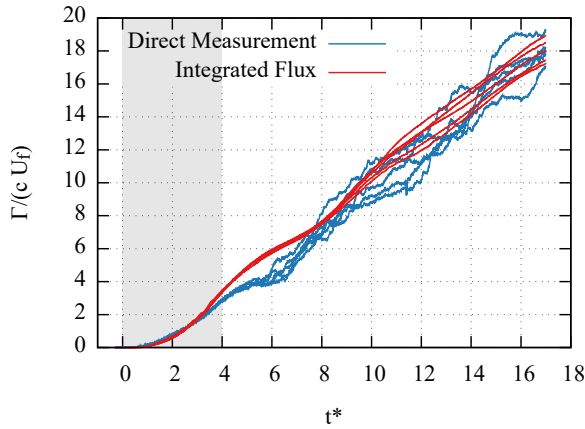

FIG. 5: Positive circulation nominally in the LEV for 5 independent measurements.

vortex formation ends due to the change in kinematics or as a result of the vortex becoming saturated with circulation. Note that the circulation production settles to a nearly constant value at later times, $t^* \geq 12$.

The amount of total positive circulation measured in the flow field, i.e. that nominally in the LEV and including that in the free wake, is shown in fig. 5 as a function of nondimensional time, t^*. The figure shows both the directly measured area integral of circulation from each PIV frame and the time integral of the leading-edge circulation production. Circulation increases monotonically with time as one would expect based on the overall state of the flow in section III A and the always-positive flux measurements. The vorticity generated at the leading edge becomes a shear layer that feeds into the LEV, continuously increasing its strength. The circula-

tion versus time curve is near linear overall, though it could be said to be more quadratic at very early times. This nonlinear variation at the start of motion is a direct consequence of the linear increase in circulation flux seen in fig. 4. When that linear function is integrated in time, a quadratic curve results. The integrated circulation production matches with the total circulation as directly measured, except for the period between $t^* = 3$ and 8. This is in opposition to the results reported by Panah *et al.* [31]. Their study found the leading edge to produce twice as much circulation as was measured directly. In that study, the difference was accounted for via their measurements of the secondary vorticity produced under the LEV, which annihilated half of the leading-edge vorticity production. The discrepancy between their study and the present work likely lies in their use of reciprocating plunge kinematics, although the underlying reasons are not entirely clear. This annihilation effect could also be the reason for the difference between measured and time-integrated circulations in the present study between $t^* = 3$ and 8, as this corresponds to a period of very strong secondary vorticity generation. (Note the negative vorticity boundary layer at these times in fig. 1.)

In summary, it has been shown that the production and subsequent transport of vorticity are important factors in the force production of the wing, and therefore are also important factors in the prediction of forces. In the following section, models from the literature will be classified and evaluated on their ability to predict the evolution of wake vorticity.

IV.   MODELING METHODS

This section evaluates the success of various models from the literature at predicting the forces experienced by a flat plate wing in the baseline case. In most previous work, model success has been judged via comparisons of qualitative images of the wake vorticity and the corresponding force production. While these are certainly reasonable metrics, they are both global flow measurements and so tend to obscure the root causes of any problems that may exist. In the current work, a closer look is taken at quantitative comparisons. Crucially, model predictions for the characteristics of the LEV, e.g. circulation and circulation production, are compared to their experimentally measured counterparts. Circulation production in particular is a good method for isolating, insofar as it is possible, the critical leading-edge condition. While it is not possible to completely separate the effect of the leading-edge condition from the rest of the flow, comparing circulation production is as close as one can come to decoupling the system. This allows for an evaluation of the Kutta condition as a leading-edge condition independent of the global flow state.

A.   Quasi-Steady and Data Driven Models

The simplest possible model of the flow over a flat plate wing is to assume that it is attached (perhaps an overly bold assumption), and that the wing is undergoing steady translation at a constant angle of attack. The start of the motion is assumed to have occurred long ago, and thus the starting vortex is considered irrelevant. The bound vortex strength (i.e., the bound circulation on the wing) is determined so as to satisfy the Kutta condition at the trailing edge,

$$\Gamma = \pi c U \sin(\alpha), \quad (5)$$

where c is the chord, U is the wing velocity, and α is the angle of attack. The quasi-steady modeling approach neglects the wake entirely. The circulation that would be shed into the wake to balance changes in the bound circulation, as required by Kelvin's theorem, is ignored. This results in the following expressions for lift, drag, and pitching moment, respectively:

$$L = \pi \rho c U^2 \sin(\alpha) + \frac{1}{4}\pi c^2 \rho \sin(\alpha)\cos(\alpha)\dot{U} \quad (6a)$$

$$D = \frac{1}{4}\pi c^2 \rho \dot{U} \sin^2(\alpha) \quad (6b)$$

$$M_b = -\frac{1}{8}\pi \rho c^2 U^2 (2b - 1)\sin(2\alpha). \quad (6c)$$

The moment, M, is given about a pivot point, b, defined as 1 at the leading edge and -1 at the trailing edge. The pivot point is usually specified at the quarter chord, $b = 1/2$, because this causes the moments that arise from wing translation and the bound vortex to cancel each other. Applying a normalization by dynamic pressure, $q = 1/2\rho U_f^2 c$, as in the experimental results and substituting $b = 1/2$ results in expressions for the coefficients of lift, drag and pitching moment:

$$C_l = 2\pi \sin(\alpha)\frac{U^2}{U_f^2} + \pi\frac{c}{2}\sin(\alpha)\cos(\alpha)\frac{\dot{U}}{U_f^2} \quad (7a)$$

$$C_d = \pi\frac{c}{2}\sin^2(\alpha)\frac{\dot{U}}{U_f^2} \quad (7b)$$

$$C_{m,c/4} = 0. \quad (7c)$$

Here, U represents the instantaneous wing velocity and U_f is the final, reference, velocity. The lift, C_l, equation has two components: the first is the circulatory contribution from the bound vortex, and the second is the non-circulatory contribution (sometimes called the "added mass" force). The drag, C_d, equation has only a non-circulatory component, and predicts zero drag in the steady state. The circulatory force component always acts in the vertical direction (i.e. lift), while the non-circulatory force always acts in the plate-normal direction but is zero in steady flow. The moment about the quarter chord, $C_{m,c/4}$, is also predicted to be zero. Equations 7 are the classic results of thin-airfoil theory (see, e.g., Anderson [51]), slightly adapted to account for a large angle of attack, a time-varying wing velocity, and non-circulatory force.

The forces given by equation 7 can easily be computed for the towing motion considered here and so compared to the measured forces. In a quasi-steady model, the flow state, and therefore the forces, can only depend on the instantaneous wing kinematics (i.e., wing location, angle of incidence, and their first derivatives in time). This makes a quasi-steady model extremely cheap to evaluate, but, as will be shown, makes it difficult to capture many of the gov-

erning physics.

Figure 6 shows a comparison of the measured plate-normal (C_N) and plate-tangential (C_T) force coefficients to the predictions of the model. It also shows the two components of the model. The circulatory lift is shown as "C_L circulatory," and the plate-normal added mass as "C_N non-circulatory." The steady-state force prediction gives the classic result of $C_l = 2\pi \sin\alpha$ and $C_d = 0$, which has been shown to compare favorably with experimental measurements on thick airfoil profiles (see, for example, Abbott and Von Doenhoff [83]), at least until stall. When the wing stalls, experimental values of the lift force are significantly lower and the drag force is significantly greater that this prediction. In the case of the current experiments, the wing is clearly stalled and the normal force is over-predicted, particularly at long times. Additionally, focusing on normal and tangential force rather than lift and drag hides the complete lack of a drag prediction in the classic result, which fortuitously cancels the over-prediction in lift to bring the predicted normal force closer to experiment. Particularly during the early part of the wing motion ($t^* = 0$ to around 2), the combination of over- and under-prediction in the model gives a result that is surprisingly close to the measured normal force, but not the tangential force.

The non-circulatory force, labeled "C_N non-circulatory" in fig. 6, is quite difficult to isolate in experiment. Potential theory predicts a force per unit depth of $F = 0.25\pi c^2 \dot{U} \sin\alpha$ in the plate-normal direction. This is a two-dimensional calculation and hence neglects any end effects, but simply multiplying by the span of the wing turns out to be essentially exact for the aspect ratios considered here, and is as confirmed in the review of added mass by Brennen [84]. In the current problem, the non-circulatory force has a characteristic top-hat shape that corresponds exactly to the acceleration profile and matches the magnitude of the initial jump in forces. Puzzling, however, is the lack of a distinct drop in the measured forces when the wing stops accelerating, at $t^* = 4$, when the non-circulatory force goes to zero.

Comparison of the quasi-steady model with the measured LEV data cannot be done in a direct fashion since the model does not include a wake of any sort. However, a general comparison can be made between the bound circulation of the attached flow model and the strength of the LEV. This may not be all that far-fetched, as it has been previously argued by Pitt Ford and Babinsky [24] that a flat plate wing at high angle of attack contains very little bound circulation, and thus any circulation that would have been bound is present in the flow as an LEV. The results of this comparison are shown in

fig. 7. Figure 7a compares the amount of bound circulation predicted by the attached flow assumption to the measured circulation in the LEV. Figure 7b compares the time rate of change of the bound circulation to the measured circulation production at the leading edge as computed from the vorticity flux leaving a box around the leading edge. In these figures, one sees the underpinnings of the circulatory force prediction, as well as the reasons for its failings. Up to $t^* = 1$ the circulation and circulation production matches reasonably well, but the predictions given by the quasi-steady model grow much faster than the measured values through $t^* = 4$, and quickly outstrip the actual circulation in the real (measured) case. The amount of circulation predicted by the model becomes constant when the wing stops accelerating and reaches its final velocity at $t^* = 4$ because the bound circulation, given in equation (5), is a function of wing velocity only.

Further, the lack of a wake causes the quasi-steady model to miss the continual production of circulation that occurs throughout the wing motion. Figure 7b shows how the model stops "producing" any circulation after $t^* = 4$, resulting in the fixed value of total circulation after $t^* = 4$. This fixed value causes the initial over-prediction of circulation to eventually become an under-prediction as the real flow continues to generate vorticity at the leading edge. This is indicative of a primary difference between steady attached and stalled flows—stalled flows require the continued production of vorticity to feed the shear layers at the edges of the plate, even in the fully developed flow. Attached steady flow reaches a fully developed state with a certain amount of bound circulation. Thereafter, attached flow does not produce any further net circulation, except in the case of unsteady motion, which will necessarily produce wake circulation to balance changes in the bound circulation.

Adding an empirical correction can mildly improve the force prediction given by the quasi-steady model, and this approach is widely adopted in the flapping wing controls community [45, 46, 85]. This approach works best for rotating wing kinematics because the attached LEV that forms there causes the force to rapidly achieve an LEV-enhanced steady state value, as seen in Manar *et al.* [86], making the quasi-steady assumption valid. Adding a bit of empirically derived foreknowledge to the quasi-steady model can be done by simply using a lookup table for $C_{l,f}$ and $C_{d,f}$ based on the steady-state time-averaged coefficients. The coefficients for the single angle of attack considered are taken from the steady state results in fig. 2, where $C_{L,f} = C_{D,f} = 1.1$. Since the current test case is fully three-dimensional, values of $C_{L,f}$ and $C_{D,f}$ (the finite wing form of
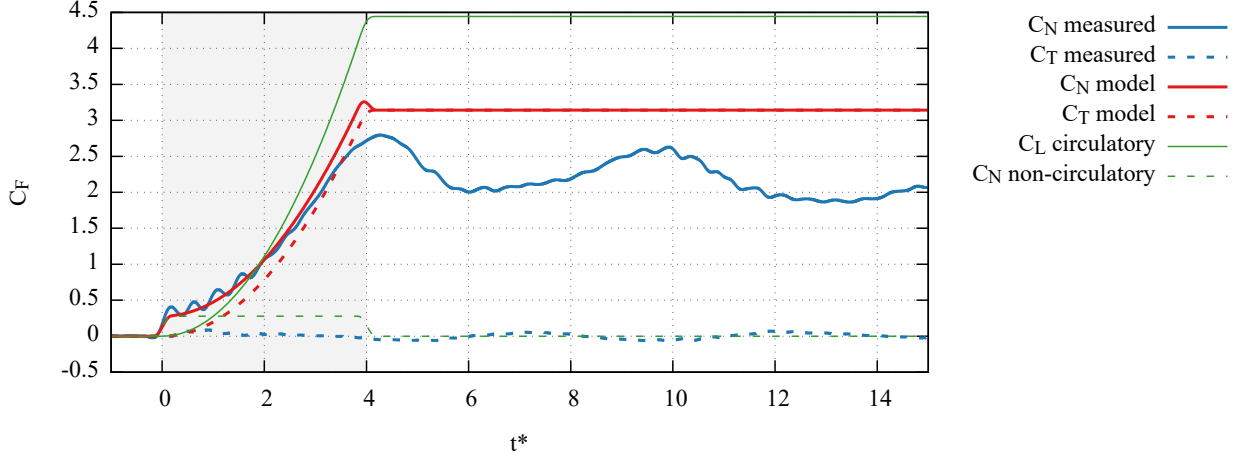
FIG. 6: The quasi-steady thin airfoil theory model force prediction compared to experimental data.

coefficients) from experiment have been used, and thus finite wing effects are empirically accounted for. The instantaneous values of the circulatory forces are then $C_L(t) = U(t)^2/U_f^2 C_{L,f}$ and $C_D = U(t)^2/U_f^2 C_{D,f}$. The same equations as before are used for the non-circulatory component, resulting in the time history shown in fig. 8. The steady state values for the coefficients are taken from fig. 2 at $t^* = 30$. The dependence on dynamic pressure gives the force transient a quadratic shape during wing acceleration (proportional to U^2), followed by a fixed value after the wing reaches its final tow velocity. Note that the C_D line has been omitted in this plot since it is identical to the C_L curve for a wing at $45°$. In the wing-fixed reference frame, using the empirical data has given the correct result of zero plate-tangential force.

To first order, the predicted and measured values of C_N, shown in fig. 8, are not all that different. Both have an initial sharp rise in force from the non-circulatory component, as well as a subsequent rise in forces during the acceleration. The model gives this as a quadratic function; the measured data has a similar shape. The model also predicts peak force near the end of acceleration at $t^* = 4$. The empirical quasi-steady model misses the magnitude of the peak by a fair margin, however, and does not capture the subsequent relaxation to steady state. It does match the forces once they have settled to steady state after $t^* = 30$ (not shown), but this is no great feat considering the empirical correction used in this data-driven approach.

The model's failure to capture the magnitude of the peak forces and their subsequent relaxation is directly related to its complete disregard of the wake. As was shown in section III A, the actual flow con-

tains significant wake vorticity dynamics, in particular the formation of a leading-edge vortex above the suction side of the wing. The presence of this vortex near the wing produces a low-pressure region that augments the force on the wing beyond what the quasi-steady model predicts. A quasi-steady model has no hope of capturing the effect of the LEV because by definition all terms related to the wake and time history have been neglected. In spite of this omission, the quasi-steady model is not a complete failure. The non-circulatory force, which does not depend on the wake, captures the initial jump in force production as the wing begins to move quite well. This is a common theme throughout the models, as the theory behind the non-circulatory force does not require any of the approximations required to capture the wake and circulatory forces.

In summary, the main attraction of the quasi-steady model is its simplicity and ability to produce reasonable results when coupled with empirical data. Its weakness, however, lies in its lack of a wake model. The next models will take the first steps towards considering the full unsteady wake.

B. Fixed Wake Model

For flows with unsteadiness, the change in bound circulation on the wing must be balanced by circulation shed from the edges of the wing. In the fixed wake model, this change in circulation is captured, but only attached flow is considered to still allow for a pen and paper solution. The second assumption taken here is that the wake sheet emanating from the trailing edge of the wing does not convect (in the lab-fixed reference frame) but is sim-

(a) Total Circulation
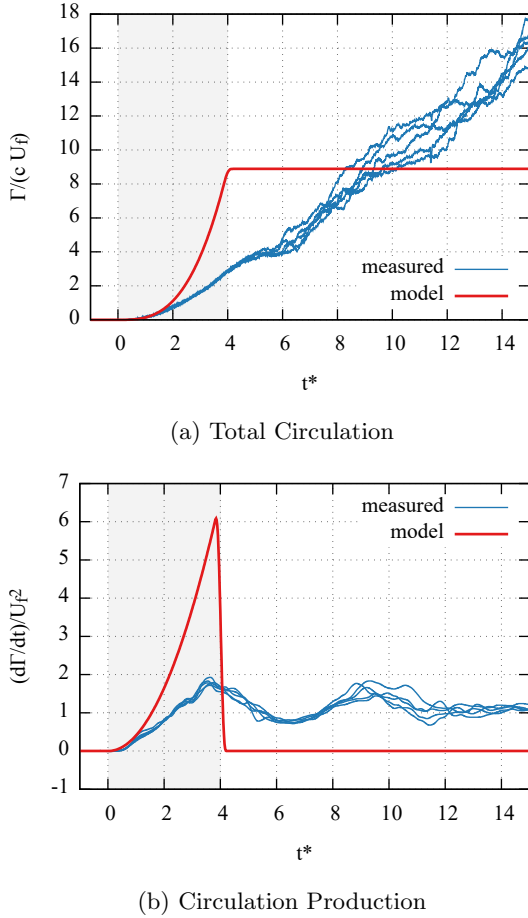

(b) Circulation Production

FIG. 7: A comparison of the circulation predicted by pure thin airfoil theory and the measured values. Note that technically the measured data is that of the LEV in the wake, while the model curves show bound circulation.

ply left behind by the wing. Using this approach produces the well-known lift deficiency function that describes the delay of circulatory force production, e.g. Wagner's model [33, 87]. The fixed trailing edge wake is the core principle behind the models of Wagner [33] and Theodorsen [35], which cover impulsive and oscillatory wing motions, respectively. Several authors have since extended on the basic principle, such as Greenberg's model of an oscillating free stream [88], Leishman's model accounting for compressibility effects [89], von Kármán and Sears's impulse derivation [87], Kussner's model for a sharp-edged gust response [90], and Sears' oscillating gust model [91]. These approaches have each been experimentally validated (e.g., in Ref. [92]) for small amplitude attached flow disturbances and enjoy widespread use. Numerical implementations of these ideas have also been used for large amplitude

unsteady motions that maintain attached flow, such as avian flapping in Hall and Hall [93] and Hall *et al.* [94]. Their work was then further extended by Salehipour and Willis [95] to find optimum flapping kinematics.

The results of applying Wagner's model to the present case are shown in fig. 9. Mathematically, this is accomplished by convolving the lift deficiency function with the bound circulation result of fig. 7a. The lift deficiency function can be found in Wagner's original work [33], or many text books, e.g. Bisplinghoff *et al.* [1]. Its basic shape is a curve that begins at one half, and then gradually asymptotes to the final value, taking on the order of twelve chords of travel to reach ninety percent of steady state. Thus the effect of convolving it with the circulation curve is to delay the growth in lift force of the wing. The plot in fig. 9 gives the same components as in the results of the quasi-steady model shown in fig. 6 and fig. 8: the measured C_N and C_T curves alongside their predicted counterparts, and the C_L circulatory and C_N non-circulatory model components. As expected, Wagner's model shows, in fig. 9, many of the same features as the quasi-steady model of section IV A. The obvious difference here is the delay in the buildup of the circulatory force. Accounting for this delay causes the model to do a reasonable job of predicting the magnitude of the normal force during acceleration ($t^* < 4$, comparing the red model results to the blue measured results in fig. 9), and instead of over-predicting the peak force just before $t^* = 5$, as in the quasi-steady case, it under predicts it. The steady state values are, as before, vastly over predicted. The alignment of the normal forces at early times ($t^* < 4$) is disingenuous however, as it neglects the plate-tangent component of force. In keeping with the Kutta-Joukowski lift theorem, Wagner's fixed wake model predicts the presence of lift with no drag. In the wing-normal and wing-tangential axes, this corresponds to equal plate-normal and plate-tangential components at $\alpha = 45°$. It is thus only a twist of fate that the normal force has nearly the correct magnitude. The plate-tangential force, which was measured at close to zero, is modeled to have the same magnitude as the normal force. Thus, in reality, the total force is predicted by this model to be much larger than the measured total force.

To see why the lift is over-predicted, fig. 10 shows a comparison of the bound circulation in the fixed wake model to the measured LEV circulation, as well as the predicted rate of change of circulation to the measured vorticity flux at the leading edge. These results show the same over-prediction of total circulation and circulation production that was seen in quasi-steady model during the acceleration portion
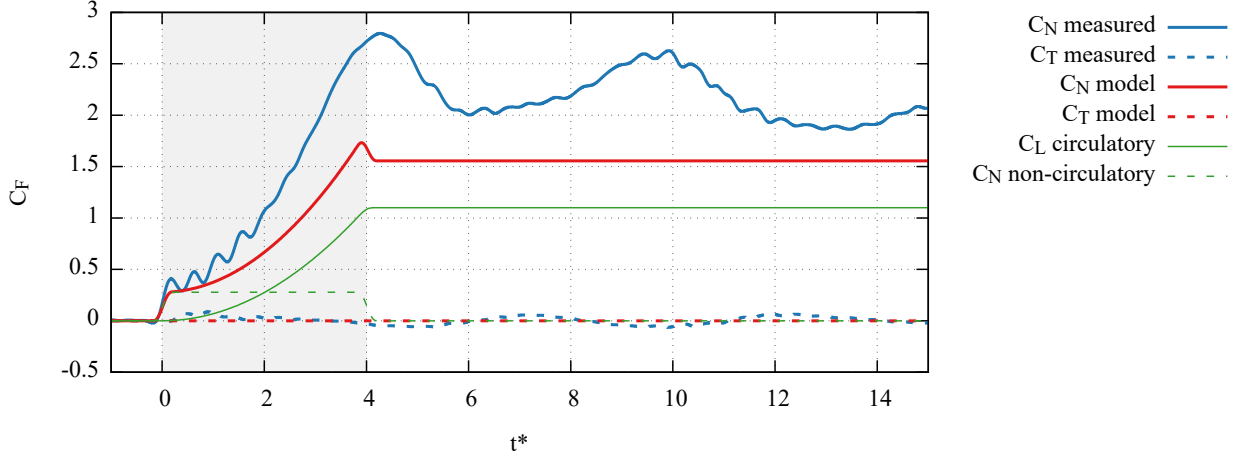
FIG. 8: The quasi-steady model augmented with empirical force coefficients and compared to experimental data.
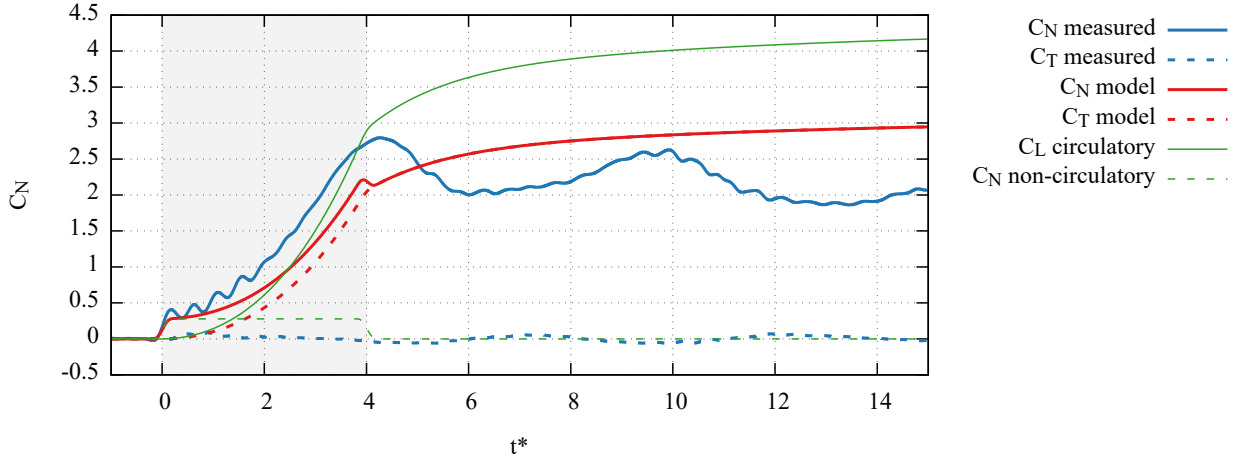

FIG. 9: The results of Wagner's fixed wake model compared to experimental results.

of the wing motion ($t^* < 4$), followed by an under prediction at steady state. The Wagner model, being an attached flow model, also shares the same deficiency as the quasi-steady model in predicting long term force behavior. Attached flow models predict a fixed total amount of circulation, while the actual stalled case continues to create circulation ad-infinitum.

However, the early portion of the circulation production ($t^* < 6$) and total circulation ($t^* < 3$) has been significantly improved in this model. Circulation production matches experimental results until $t^* = 2$, and the decay of production after the end of acceleration ($t^* = 4$ to 6) at least has the correct shape. This is a good sign that the addition of a wake to the flow model has improved the overall quality of the prediction despite the gross simplifi-

cation of that wake model.

C. Similarity Solution

To further improve on the solution offered by the fixed wake model, the convection of the vortex sheets due to both the wing's velocity field, and the effect of the wake on itself, needs to be considered. A general solution is analytically intractable, but for simple cases a similarity solution to the shape and strength of the vortex sheets shed from a sharp edge can be found. This is the idea behind the work of Pullin [96], who proposed a truncated series solution for a vortex sheet shedding from the end of a semi-infinite plate in cross-flow. Pullin and Wang [36] applied that solution to a finite plate, and showed that to a
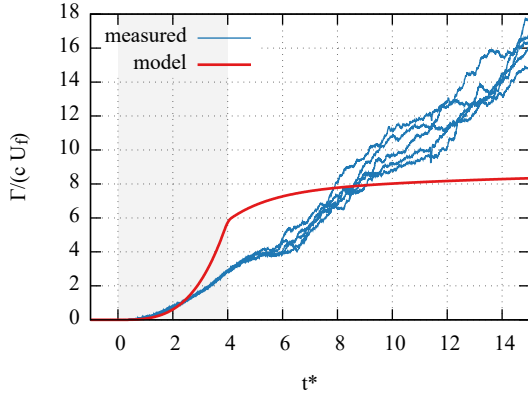
(a) Total Circulation
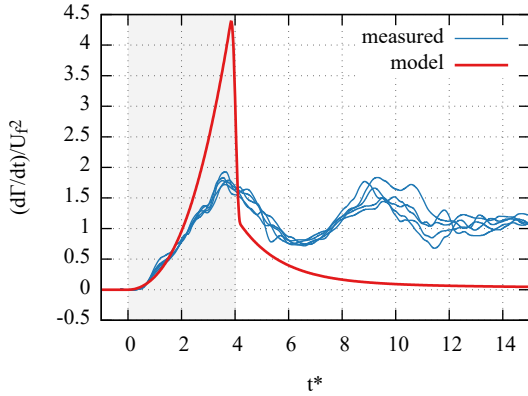
(b) Circulation Production

FIG. 10: A comparison of the circulation predicted by Wagner's model and the measured values. Note that technically the measured data is that of the LEV in the wake, while the model curves show bound circulation.

first-order approximation, the leading- and trailing-edge vortex sheets do not influence one another.

To make an analytical solution of the wake sheet tractable, Pullin's similarity models assume a wing velocity profile with a simple polynomial dependence on time:

$$U = Bt^m \qquad (8)$$

where B is a scaling factor and m determines if the profile is of constant speed, constant acceleration, etc. The flow is assumed to be quiescent at $t = 0$. For comparison to the present work, a constant acceleration profile of $m = 1$ was used. The value of B was set to match the velocity profile modeled here to that of the experiments, resulting in $B = 0.25$. Choosing a constant acceleration profile immediately limits the applicability of this model to only

the acceleration portion of the test (i.e. $t^* <= 4$), as it cannot accommodate the change to constant velocity.

The equations for force on a flat plate wing starting from rest given in Pullin and Wang [36] break down into two components: a non-circulatory and a circulatory component. Both force components have only a plate-normal term, as meeting the Kutta condition at both plate edges removes any possibility of plate tangential force (i.e., edge suction). The notation from their paper has been modified to fit the notation used here. The non-circulatory component is purely plate-normal, and is given as:

$$N = \frac{1}{4}\pi c^2 \rho \sin(\alpha)\dot{U} \qquad (9)$$

where N is the plate-normal force, and all other quantities have the same meanings as before. This matches the non-circulatory force used previously in equation (6), albeit written as a plate-normal force rather than decomposed into lift and drag.

The circulatory component, also purely plate-normal, is the heart of the model. Using the simplified velocity profile given in equation (8), the evolution of the shed vortex sheet can be represented by an infinite-series similarity solution based on Kaden's spiral. The leading term of the series is then solved for to give the shape of the rolled-up vortex sheet. In the course of the derivation, given in Ref. 36, it is also argued that the effects of the plate-tangent velocity component only enter the problem as higher order terms of the series and are thus neglected. The resulting equation for the circulatory force is given as

$$N = \frac{2}{3}(5m + 2)K\rho c^{1/2} J_0 a^{5/3} t^{\frac{5(1+m)}{3} - 2}\Re\left\{\omega_0^{1/2}\right\} \qquad (10a)$$

$$a = c^{1/2} B \sin(\alpha) \qquad (10b)$$

$$K = \left[\frac{3}{4(1+m)}\right]^{2/3} \qquad (10c)$$

where N is once again the normal force, and a and K are convenient scaling factors. The values of ω_0 and J_0 represent the similarity solution shape and circulation, respectively, of the rolled-up vortex sheet and are non-analytical functions of m. Their values are taken, as in Pullin and Wang [36], from the numerical solution in Pullin's previous work [96], and are $\omega_0 = -0.17 + 0.33i$ and $J_0 = 2.185$. A series expansion for circulation of the LEV is also given in
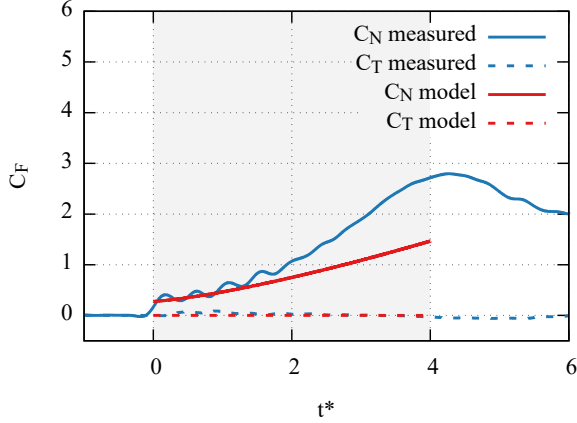
FIG. 11: The similarity solution model compared to experimental data.

Ref. 36, which to leading order is

$$\Gamma = \frac{\delta_0^2(t)}{K^{3/2}t}J_0 \tag{11a}$$

$$\delta_0(t) = Ka^{2/3}t^{2(1+m)/3} \tag{11b}$$

where δ_0 is another intermediate scaling factor. The rate of circulation produced by the accelerating wing is the time derivative of the expression for Γ.

These equations for force are based on solutions for both the shape and circulation of the wake sheet that satisfy only the leading term in an infinite series, and thus accuracy is expected to be limited to short times. In addition, it is worth noting that making the solution analytically tractable required Pullin and Wang to ignore the effect of the LEV on the TEV and vice versa, although this was shown to be a second-order effect for the short times of interest.

Results from implementing Pullin and Wang's similarity model are given in fig. 11, where they show agreement with the experimentally measured results through $t^* = 2$, after which time they predict a smaller plate-normal force than was measured. This is the expected result based on conclusions in Pullin and Wang's paper [36]. A reason for the under-prediction of the forces can be found in the circulation prediction given in fig. 12. The total circulation is predicted reasonably well for $t^* < 1.5$, but does not scale properly with time, and does not adhere to the linear growth of the experimental measurements. This results in under-predicted circulation and force values at longer times. At short times, the difference in shape between the measured and predicted circulation productions is likely due to the model's ignorance of the smoothing used for the experimental velocity profile. (Recall that the model requires
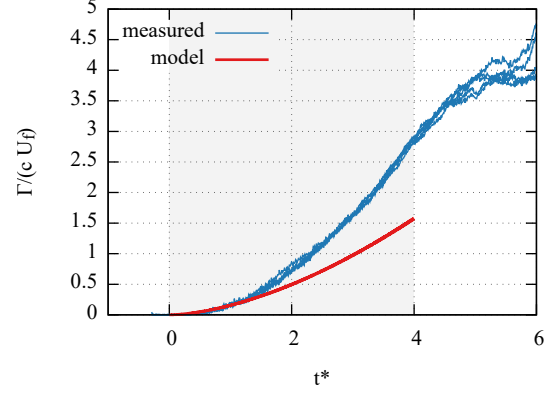
(a) Total Circulation
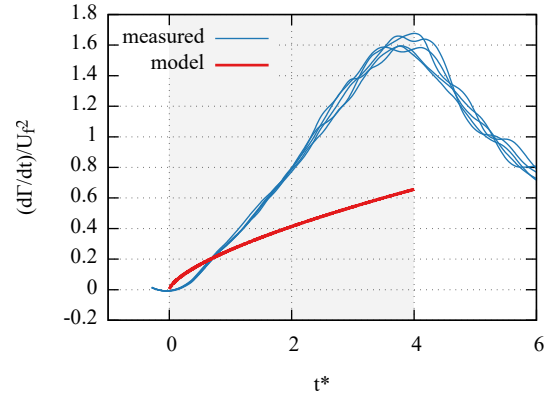
(b) Circulation Production

FIG. 12: A comparison of the circulation predicted by the similarity solution model and the measured values.

a very simple exponential velocity profile definition.) At longer times ($t^* > 0.25$) the mismatch is likely due to neglecting the higher order terms, particularly those that deal with the velocity induced by the LEV on TEV and vice versa.

In spite of its shortcomings, the similarity solution model presents a closed form solution to the separated flow that correctly predicts the lack of plate-tangential force. In doing this, the model provides valuable insight into how the flow behaves at early times. This model also serves to illustrate the limits of what a purely analytical solution is capable of capturing. While the assumption of no LEV-TEV interaction in the Pullin and Wang model produces viable results for short times, even at moderate times the interaction must be captured in order to accurately model the resulting force production. Furthermore, the similarity solution model is not capable of dealing with anything except single-term polynomial velocity profiles. In order to implement a more general

solution method, Pullin admits, and this author concurs, that a numerical procedure must be used [96]. While the similarity solution model's stand-alone use may be limited, it is quite useful in its capacity as a method for kick-starting more general numerical methods (e.g., those in Refs. 21, 40) by providing a solution to the early, nearly singular, vortex behavior.

D. Two-Vortex and Impulse-Matching Models

To combat the growth in computational cost and bridge the gap between numerical and analytical models, Wang and Eldredge [21] extended the work of Cortelezzi and Leonard [97] on modeling unsteady separated flows with point vortices that have time-varying strengths. In this approach, the wake is represented by a very small number of point vortices (i.e., one for each shedding edge) whose strengths change in time to maintain the Kutta condition as the vortices convect downstream. This constitutes a wake model that captures the effect of flow separation from both edges while keeping the degrees of freedom to an absolute minimum, making it an extremely computationally efficient modeling technique.

The results of applying this two-vortex model to the present case are shown in fig. 13. The figure shows the measured forces in the wing-relative reference frame, C_N and C_T, compared with predictions given by a two-vortex model. It also shows the model's circulatory and non-circulatory components independently. The two-vortex model correctly captures the lack of plate-tangential force, but over-predicts the strength of the plate-normal force by almost a factor of two. The non-circulatory forces are captured in exactly the same manner as in the previous models, with similarly successful results. The discussion will thus once again focus on the circulatory force contribution from the wake.

The force history in fig. 13 does not extend past $t^* = 5$ because the simulation becomes unstable. In certain configurations, it happens that the vortices have little ability to enforce the Kutta condition at the edges. This leads to large changes in circulation for small changes in vortex location. When coupled with the Brown-Michael convection scheme [98], which alters the vortex velocity to account for circulation change, these two effects feed back into each other and cause a divergence of vortex strength and location. The initial stages of divergence can be seen in the squiggles of rapidly increasing magnitude at the end of force curves in fig. 13.

It was initially assumed that the over-prediction of force observed in the comparison of the two-vortex model to experimental results stemmed from enforcement of the Kutta condition at the leading edge. Either the Kutta condition was an incorrect, overly aggressive, choice for the leading-edge boundary condition, or using a point vortex far from the shedding edge lead to overzealous addition of circulation. The effect of a point vortex falls off with $1/r$, so to maintain the same condition at the edge, the vortex strength must increase faster for lone shed point vortices than if a shear layer was included. However, the measured circulation data in fig. 14 shows that the strength of the LEV is captured by the model. The expected effect of the point vortex receding from the wing is seen in the increasing overshoot of the modeled circulation production after $t^* = 3$. Better, in fact, than the force data, which rapidly diverges from the measurement for $t^* > 1$. Based on the prediction of LEV circulation, one would expect reasonable force predictions through at least $t^* = 2$.

Note that there is some noise in the circulation flux just after the start of the wing motion. This is associated with the leading-edge vortex not being placed in quite the correct location by the initial conditions and the time step being too large to handle to nearly singular velocity close to the plate edges in the circle plane. The noise quickly settles out as the vortex moves away from the singularity, and the initial placement has only a small effect on the overall outcome.

Since circulation appears to be predicted reasonably well, the error in force prediction must come from elsewhere. The answer lies in the location of the vortex. The model predictions for LEV location are shown in fig. 15. The two subfigures show the x/c and y/c values obtained from the two-vortex model, as well as experimental measurements in which the vortex is identified using both the vorticity centroid and Γ_1 criteria. While the modeled x/c location of the LEV is on the right track with respect to the experimental results, the two-vortex model predicts a lower value of horizontal displacement than the measurements, indicating that the model represents a LEV that is closer to the wing than observed in experiments. The trend in y/c location as predicted by the model is backwards, indicating an LEV that rises above the leading edge of the wing, rather than one that sinks below it. Incorrectly predicting the location of the LEV has a direct impact on the force experienced by the wing.

Note that the location of the vortices also impacts their circulation as the vortex strengths are updated each time step to continue enforcement of the Kutta condition. As the vortex moves further away from the plate its image approaches the center of the cylinder, and thus is never more than a cylinder radius away from the edge. Therefore the
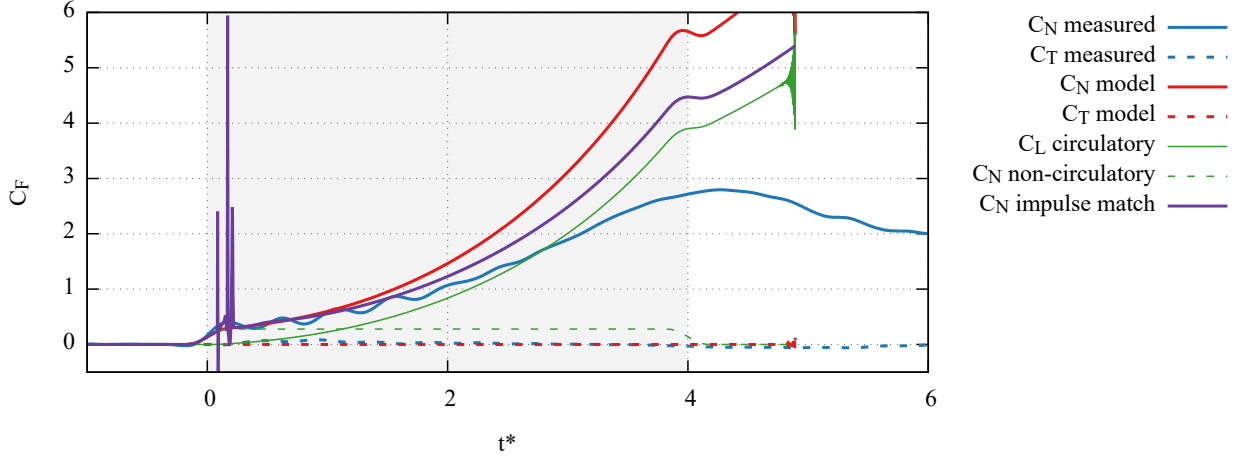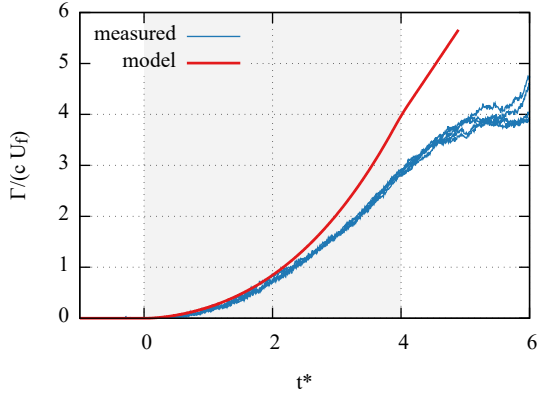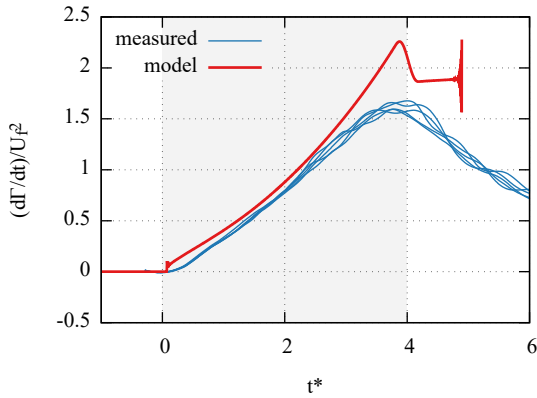
FIG. 13: The Wang and Eldredge point vortex model.

(a) Total Circulation

(b) Circulation Production

FIG. 14: A comparison of the circulation predicted by Wang and Eldredge's model and the measured values.

image vortex, rather than the vortex itself, accounts for the majority of the induced velocity at each edge. Furthermore, since the image moves relatively little, the location of the vortex actually has a diminishing impact on its own circulation as the vortex recedes from the plate. The force produced by the vortex pair however, is independent of vortex location.

Wang and Eldredge [21] were aware of the incorrect convection, and the second thrust of their paper was to propose a new model for convection that moves the vortex so as to cancel the effect its motion has on the total force. As an added benefit, the impulse-matching model allows arbitrary choice of vortex shedding time. The results of switching to their new "impulse matching" convection scheme are shown in fig. 13. Applying the impulse matching convection improved the force, but did not entirely eliminate the problems already noted.

The two-vortex wake model is extremely attractive from a conceptual and computational cost standpoint, but is unfortunately hamstrung by its over-simplified wake representation. The key omission appears to be the effect of the shear layers that form at the leading and trailing edges of a wing in viscous flow. These shear layers are where the roll-up of new vortices occurs; without capturing their dynamics either an additional ad-hoc vortex shedding relationship must be added or coherent vortex shedding forgone altogether. These deficiencies would merely limit the model to short times if it were not for its gross overestimation of the forces. This shortcoming has been recognized by the Eldredge group, and an extension of the present model that includes the shear layer has been proposed [99]. In summary, the two-vortex model presented here shows great promise for relatively short times when the flow is dominated by the initially shed LEV and
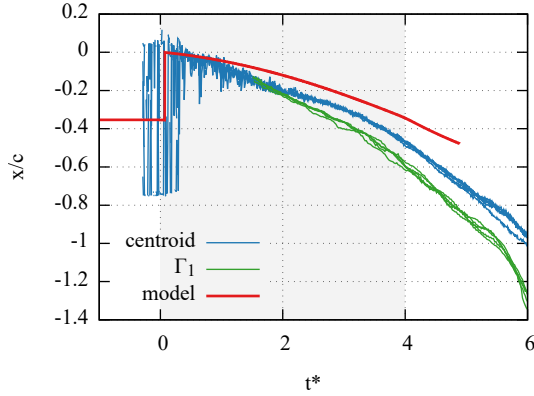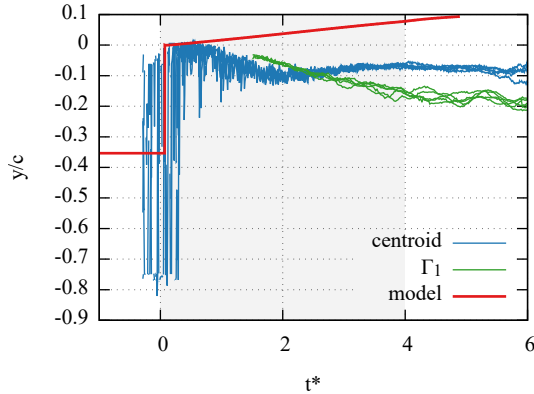
(a) LEV x/c

(b) LEV y/c

FIG. 15: A comparison of the location predicted by Wang and Eldredge's model [21] and the measured values.

TEV. For the flapping wing applications, for example, this may be all that is required before the wing reverses course.

E. Multi-Vortex Model

Lagrangian multi-vortex methods present themselves as an attractive option to solve the problem of wake convection in a more holistic way. Allowing the wake to convect with the flow leads to the roll-up of the shear layers at the leading and trailing edges and the formation of the leading- and trailing-edge vortices. This natural inclusion of the wake evolution has made Lagrangian vortex models a popular choice, and many examples exist in the literature including Katz's thick airfoil method [42], Xia and Mohseni's conformal mapping method [56], Ansari *et al.* 's strip theory approach for 3D wings [41, 57], and Hammer *et al.* 's work [20], to name but a few.
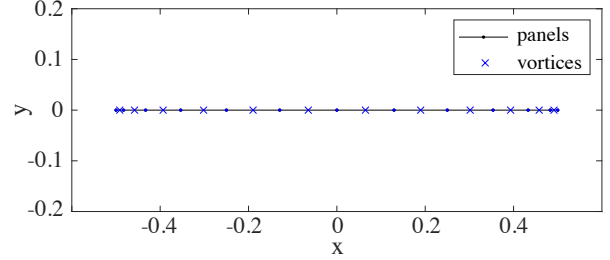

FIG. 16: A representative panel method mesh with $N = 12$. The actual computations used a finer mesh where $N = 64$.

The method implemented for the present work is similar to the one outlined by Katz and Plotkin [52]. The wing is represented by $N = 64$ point vortex panels, with cosine spacing across the chord, depicted in fig. 16. Each panel contains a point vortex at the panel center; collocation points are at the panel edges. This setup places collocation points exactly at the plate edges and thus implicitly satisfies the Kutta condition at both edges. The addition of two new vortices each time step models the shedding of circulation. For the first time step, these vortices were placed a distance of 2% of the chord away from the shedding edge. The exact location of the initially shed vortex was found to have little impact on the results. In subsequent time steps, new vortices were placed at a third of the distance from the shedding edge to the previously shed vortex, as per the method in Ansari *et al.* [41]. The time step size was selected to be $t^* = 0.015$ as in Xia in Mohseni [56].

The net result at each time step is $N + 2$ vortices to solve for no through-flow at $N + 1$ collocation points. The system is closed by specifying zero total circulation. This method enforces the Kutta condition by meeting the plate-tangent shedding velocity at the edges. Vortex locations were evolved in time with an explicit Euler scheme. A vortex core model was not used so that an off-the-shelf fast multipole solver, FMMLIB2D [100], could be employed. Forces were computed with the impulse method of Wu [101]. As a final consideration, the model used a linear trapezoidal velocity profile rather than the smoothed version used in experiment.

The downside of using a panel method for body representation is that it becomes difficult to separate the resulting force into the circulatory and non-circulatory components. This could be remedied by instead representing the plate via conformal mapping as in Xia and Mohseni [56], though the point vortex panel method was selected in this case for its extreme ease in calculating the forces from the vortex impulse.

By continuously shedding vorticity from the wing,

(a) Multiple-vortex model

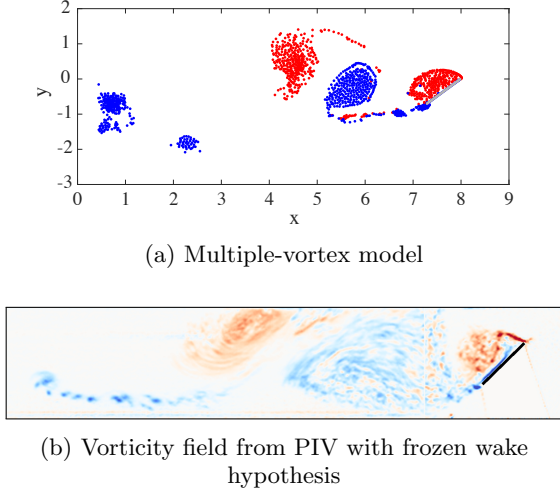(b) Vorticity field from PIV with frozen wake hypothesis

FIG. 17: Wake comparison at $t^* = 10.0$

the shear layers at both edges of the wing are more properly captured. Furthermore, allowing the vorticity to convect naturally results in the roll-up and shedding of large-scale vortices. As seen in fig. 17, the resulting wake compares favorably with the experimental frozen wake result. Using a large $(\mathcal{O}(10^3))$ number of vortices also captures the effect of the spatial extent of shed vorticity. In summary, Lagrangian multi-vortex models make for a relatively well resolved wake compared to the previously discussed methods, albeit at the expense of mild additional computational cost, which may be more expensive than some models but is still significantly cheaper than full CFD.

The force results from the multiple-vortex model are shown in fig. 18. The first feature of note is that the model correctly predicts the lack of plate-tangent force. The second important feature is that the shape of the measured force histories is captured fairly well. The model correctly predicts the peak force connected with shedding of the first LEV around $t^* = 5$, as well as the second force peak due to the formation of a second LEV around and after $t^* = 8$. The magnitude of the force is, however, not perfect. In particular, the minimum at $t^* = 7$ is under-predicted and the model over-predicts after $t^* = 8$.

The total circulation and leading-edge circulation production as predicted by the multi-vortex model are shown in fig. 19. The model does a remarkable job of reproducing the leading-edge circulation production, especially through $t^* = 6$. The minimum at $t^* = 6$ and second maximum at $t^* = 9$ are not as accurately resolved. The success in matching the circulation production carries over to the total circulation which falls well in line with the measured val-

ues outside of a slight over-prediction between $t^* = 5$ and 6. A salient point to make here is that the Kutta condition performs well at the leading edge in spite of earlier misgivings. It appears that the Kutta condition is both valid and useful for determination of leading-edge shedding for thin wings.

The question that now arises is how the circulation production can be well-predicted throughout the wing motion, but the forces less so. This is perhaps because the truly two-dimensional model is being compared with three-dimensional experimental results that were obtained on a finite aspect ratio wing. When two-dimensional measured force data is available, two-dimensional multi-vortex models have been shown to accurately reproduce the force histories [20, 44, 102].

If some method for determining when shedding should or should not occur from the leading edge were included, the present calculations could also be improved to account for more general kinematics, such as low angles of attack, pitching, and oscillation. In a low order model such as this, such a determination is generally left to ad-hoc methods such as the leading edge suction parameter (LESP) [44], a flow angle limit [102], or a simple force limit [81].

The necessary leap to make the discrete vortex methods considered in this section a complete answer to the full flapping wing problem is to extend these methods into the third dimension, but this seems to exist only rarely in practice (e.g. Roccia *et al.* [71]). It appears that fluids researchers who seek fundamental understanding of separated flows tend to overlook discrete vortex models because they stray too far from pen and paper models into numerical methods, and thus offer little insight into the origin of forces. Nevertheless, the results presented here, and others in the literature, show that computational methods like the present two-dimensional discrete vortex model can be excellent tools for determining the force on a two-dimensional profile under arbitrary motion.

V. CONCLUSIONS

The first portion of this paper has examined experimental measurements of the bulk wake characteristics of a flat plate wing at high angle of attack starting from rest. These measurements focused on the process of circulation generation at the leading edge of the wing. The second portion of the paper presented the implementation of several of the pertinent models from the literature and compared the results of these models to the experimental results.

Section III examined a single experimental test case in which an aspect ratio eight wing was held
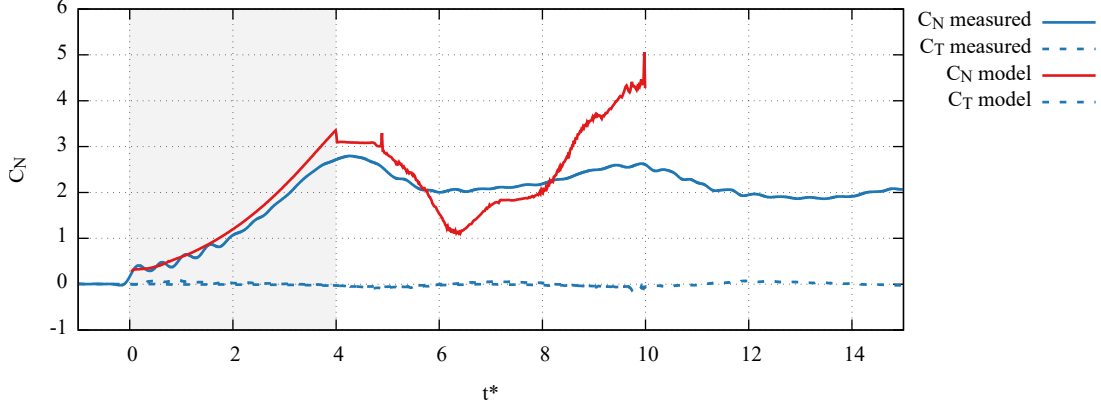
FIG. 18: The point vortex model compared to experimental data.

at a 45° angle of attack and accelerated from rest to a Reynolds number of 12,500 over a distance of two chord-lengths. The experimental results included two-dimensional flow visualization, time-resolved force measurement, vortex tracking and circulation measurement, and time-resolved leading-edge circulation measurement. The analysis presented here showed how even this relatively simple case exhibits complex and interconnected wake dynamics. It also exposed leading-edge circulation production as the critical element of the wake system, and thus highlighted the need to understand the wake dynamics in order to understand the forces on the wing.

The next section, section IV, presented an analysis of the strengths and weaknesses of various physically based models to test their ability to predict the forces experienced by the rapidly accelerated wing. These models included (in increasing order of wake fidelity) a quasi-steady attached flow model, a data-driven quasi-steady model, Wagner's fixed wake model, Pullin's similarity solution for separated plate flow, a two-vortex convected wake model, and a multiple vortex convected wake model. A comparison of the plate-normal forces predicted by these models, as well as the measured force history, was given in fig. 20. Of the models selected, only the last three account for shedding at both plate edges.

The force predicted by the models studied here can be split into non-circulatory (sometimes called "added mass") and circulatory components, though whenever invoking such a conceptual divide, it is important to remember that it is a purely conceptual one. In an actual experiment, such a distinction does not exist and there is only pressure and skin friction due to the flow as a whole. The concept of a non-circulatory force arises purely as a separation of the terms in the potential flow equations. It is, however,

useful at a conceptual level for intuitively predicting the response of the wing. The non-circulatory force component of all of the models shown here was able to successfully predict the initial acceleration-dependent jump in forces at the start of the motion. This led to the conclusion that forces due to plate motion can be considered superimposable on the circulatory forces regardless of the wake state. Further, these forces are well-captured in present models described in the literature. The circulatory components, however, account for the action of the wake. These require a case-by-case analysis, as each model uses a different method of representing the wake.

The attached flow models examined here (i.e. the "quasi steady" models and Wagner's "fixed wake" model in fig. 20) do not include adequate wake models, and were unable to predict the unsteady forces produced by the rapidly accelerated wing on all but the most rudimentary levels. The excess of predicted force was found to be due to additional circulation erroneously present in the flow. The surplus in bound circulation stemmed from enforcing attached flow on the plate where, in reality, the flow separates from the leading edge. The attached-flow assumption also leads to an incorrectly predicted plate-tangent force of magnitude equal to the normal force. These problems could be alleviated by using empirical values of the lift and drag coefficients, as in the data-driven model, but even this approach still neglects the extra forces produced by the formation and shedding of the initial LEV.

Pullin's similarity solution model, labeled "similarity" in fig. 20, presents an analytical method for obtaining the force on the plate, including the effect of leading-edge separation. The addition of vorticity shedding from the leading edge brought the direction of the predicted force in line with the measurements, i.e. this model predicted only the plate-normal force

(a) Total Circulation
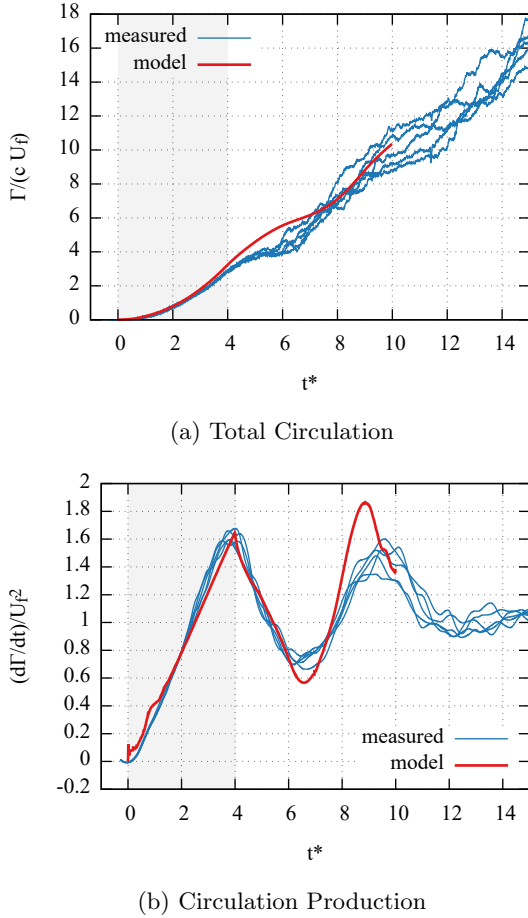

(b) Circulation Production

FIG. 19: A comparison of the circulation predicted by the point vortex model and the measured values.

to be nonzero. Ignoring higher order terms limits the model's applicability to a short time window after the start of the motion.

Wang and Eldredge's two-vortex wake model [21], labeled "two vortex" in fig. 20, uses point vortices of changing strengths to enforce the Kutta condition at both plate edges. It was found to predict the production of circulation at the leading edge well, at least until the end of the wing's acceleration, but over-predicted the forces on the plate by a factor of two or more. The error in force prediction was traced to the model's incorrect convection of the LEV when compared to experiment, and the instantaneous motion of newly produced circulation from the shedding edge to the vortex.

The multiple vortex model includes shedding from both plate edges, accomplished by adding a vortex to the wake at each time step. The wake vortices are then convected with the background flow while keeping its strength fixed. This model enforces the Kutta condition at both plate edges, and was found to give

excellent agreement with the measured leading-edge circulation production. The magnitude of the normal force was over-predicted with respect to experiments, especially after the first LEV sheds ($t^* > 8$). The fully convected wake included here allows this model to accurately capture the timing of LEV shedding and reformation, something that was not seen in any of the other models. Given the success of the circulation predictions, the failures in predicting forces must be due to other factors such as vortex convection or wake distribution.

In addition to evaluating each of these models independently and with respect to each other, another purpose of this work was to assess the validity of applying the Kutta condition at the leading edge. Earlier work and intuition have cast doubt on the validity of the Kutta condition at the leading edge based the observed lack of flow leaving tangent to the flat plate wing. The models examined here that included leading-edge separation all used the Kutta condition at the edge, and were all, within limits, successful at predicting the circulation in the LEV. The present analysis thus leads to the conclusion that the Kutta condition, despite earlier misgivings, is both valid and useful at the leading edge for high angle attack flows ($\alpha > 30°$). Errors in the model force predictions appear to come from other sources, such as the discretization or the convection of the wake.

Appendix: Experimental Methods

This section gives a description of the experimental methods and subsequent data analysis used to produce the results in the present experiments. The experimental methods very closely followed those of Manar and Jones [103], and further details can be found there.

The experimental facility used was the 1 m deep, 1.5 m wide, 7 m long towing tank at the University of Maryland. In brief, the tow motion is provided by a carriage above the tank, which connects to the wing with vertical plunge rods. The force balance and subsequent wing mount were located on the end of a horizontal sting to provide a separation of two chord lengths between the wing the plunge rods. The wings used for these experiments were flat alu-
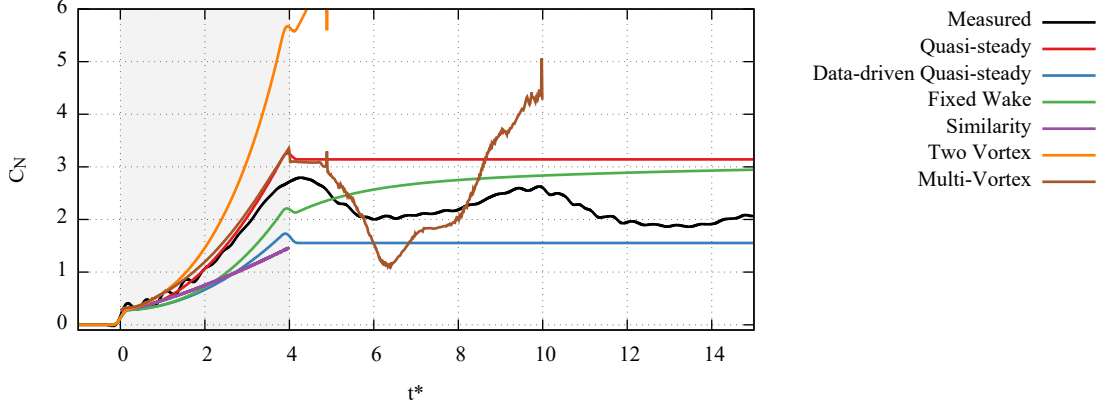
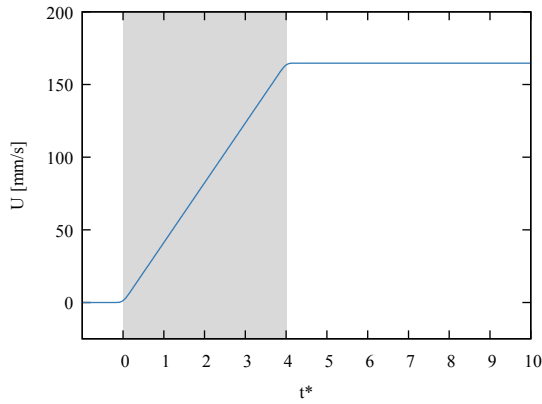FIG. 20: The normal force predictions from all models.

FIG. 21: The velocity profile of the motion.

minum plates. They had a chord, c, of $76.2\,\text{mm}$ ($3\,\text{in}$) and thickness, t, of $3.175\,\text{mm}$ ($1/8\,\text{in}$) for a thickness-to-chord ratio of $t/c = 0.042$ and an aspect ratio of $AR = 8$.

The experimental work discussed here makes use of a piecewise linear towing velocity profile consisting of a constant acceleration portion followed by a constant velocity portion. The corners (start and end of acceleration) of the plate's velocity versus time profile were smoothed slightly to minimize unnecessary vibrations in the model from rapid changes in the driving force applied. Smoothing was accomplished with a 7th order polynomial in velocity, so that velocity, acceleration, and jerk could be matched at either end of the smoothing segment. The smoothing segment was centered at the corner and was set to last 20% of the acceleration time. The velocity profile is shown in fig. 21.

The motion is set to start at $t_1 = 0$ for convenience. The final velocity of the wing is specified using the chord-based Reynolds number, $Re = U_f c/\nu$,

where U_f is the final wing velocity, c is the wing chord, and ν is the kinematic viscosity of the fluid (water in this case). The level of acceleration is specified by the distance traveled during the acceleration interval: 2c.

Time-resolved loads were measured on the wing at $1000\,\text{Hz}$ using a submersible ATI Mini40 force/torque transducer. The resulting signals were smoothed with a Savitzky-Golay filter with a width of 0.25 seconds and then ensemble-averaged over five trials.

In order to make quantitative statements about the evolution of the wake behind the wing, particle image velocimetry (PIV) was used to measure the time-resolved velocities of the flow. The PIV flow fields were analyzed to track three LEV-related quantities: the vortex location, the vortex circulation, and the circulation production at the leading edge of the wing.

The planar PIV tests were performed using a double-pulsed Nd:YLF laser (Litron LDY304, 30 mJ/pulse, 10 kHz max), with the laser sheet oriented in the chordwise direction. Soda-lime glass spheres with an average diameter of 34 μm were used as the tracer particles. Images were acquired using a Phantom v641 camera (4 MP CMOS sensor, up to 3.2 kHz at max resolution) placed orthogonal to the laser sheet and tank wall. After a sliding background subtraction to increase the signal-to-noise ratio, correlation was performed in DaVis v8.1 using multi-pass interrogation with 50% overlap. A median filter was then applied on 3×3 pixel regions, replacing vectors whose peak ratio (the ratio of the highest correlation peak to the second-highest correlation peak) was less than 2 with an interpolated velocity vector. The measurements were taken at a chord-wise plane one chord length from the center of the wing span and were ensemble-averaged over five
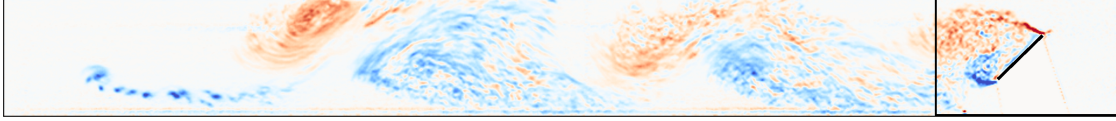
FIG. 22: The results of applying the frozen wake hypothesis. The extent of the actual PIV frame is shown to the right of the vertical black line.
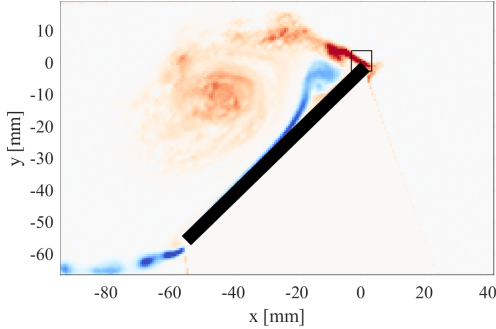

FIG. 23: The location of flux measurement marked by the black box around the leading edge.

trials.

To assess whether the PIV recordings had sufficient spatial resolution to measure the vorticity flux across the relatively small shear layer, measurements with two different fields of view (FOV) were taken of several different repetitions of the same case. The tight field of view was processed with a 24-pixel window and 50% overlap, resulting in a vector spacing of 0.84% of chord. The wide field of view was processed with a 32-pixel window and 50% overlap, resulting in a vector spacing of 1.90% chord. Thus the tight field of view has about half the vector spacing as the wide field of view (the chord is 76.2 mm for both cases).

The LEV circulation was directly computed as the area sum of the positive vorticity over the entire PIV frame. In order to still maintain a distinction between the LEV and TEV, the vorticity was split into positive and negative regions and integrated separately. This required the use of a threshold to remove the background noise. To ensure that a proper threshold was used, a sensitivity study was conducted that that showed that if a large enough threshold was used, then the measured quantities were nearly independent of the threshold. A threshold value of normalized vorticity $\omega_{thresh} = \omega c/U_f = 2.5$ was selected as a conservative result from the sensitivity study, and was 5 standard deviations above the background noise level for all cases.

The vortex location was tracked using two methods: the Γ_1 criteria and via the single-sign vorticity centroid. The Γ_1 criteria is the same from Graftieaux *et al.* [104], with a threshold value of 0.6. To further improve robustness, the centroid of the first region leaving the leading of the wing and satisfying this threshold was computed and this point was taken as the location of the LEV. For the vorticity centroid, the vorticity field was split into positive and negative regions along the same lines as the circulation measurement and the first moment of vorticity was calculated.

One of the limitations of the PIV setup is that the camera moves with the wing, and thus the wake is continually convected out of the frame. To alleviate this, the vorticity leaving the frame is assumed to be frozen in place, forming a first order approximation to the wake as a whole. The results of this approach can be seen in fig. 22. It allows for a reasonable estimate of the total circulation and centroid of vorticity throughout the entire test run in spite of the wake leaving the frame. Figure 22 also shows the alternating LEV and TEV shedding that occurs.

The frozen-wake approximation is implemented by adding a small strip of vorticity at the exit of the PIV frame onto a stationary background grid, which maintains a running average of the contribution from all frames. Obviously, this approximation is far from perfect. The vorticity in the wake that would normally convect does not, leading to erroneous locations of the shed vortices, and any vorticity that leaves through the top and bottom of the frame is neglected. Furthermore, vortices that slowly leave the frame become stretched in the fixed-wake representation. Despite the disadvantages, making the fixed-wake approximation is a vast improvement over simply neglecting the wake that has left the frame.

The production of circulation at the leading edge was measured via the flux of vorticity out of a control volume around the leading edge of the wing. The extent of the control volume is depicted in fig. 23, and is $0.08c$ on a side centered at the upper corner of the leading edge. Along the edge of the box, the vorticity flux was computed with the standard integral

$$\frac{\mathrm{d}\Gamma}{\mathrm{d}t} = \int_s \omega \vec{u} \cdot \hat{n} \, \mathrm{d}s \qquad \text{(A.1)}$$
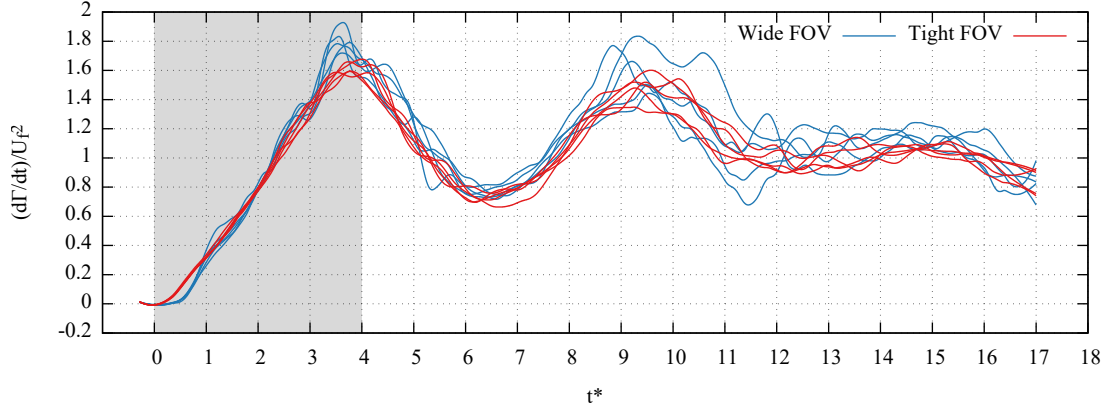
FIG. 24: Flux measurements for the two different fields of view. Note that each field of view is represented by five independent trials.

where $d\Gamma/dt$ is the vorticity flux (expressed as the rate of circulation), ω is the vorticity, and $\vec{u} \cdot \hat{n}$ is the velocity component normal to the boundary, s. The vorticity is computed with a three-point central differencing scheme in each direction. The integral is discretized with the PIV vector spacing and computed numerically with the trapezoid rule. This method measures the circulation flux slightly behind the leading edge. Doing so was a conscious choice to avoid using vectors whose correlation might be contaminated with stationary wing pixels.

The impact of the two different fields of view on the flux measurement is shown in fig. 24. The effect of halving the measurement resolution is primarily to add noise to the measurements with the wide field of view, and secondarily to impart a slightly higher magnitude for the wide FOV. The wide field of view also has a slight delay in the start of the measurement compared to the tight field of view. This was due to the measurement plane being displaced slightly further behind the leading edge in the wide field of view to ensure that it captured the whole shear layer. The wide field of view also reports a slightly higher initial peak in the flux measurement. Overall, the two methods report the same trends and magnitude of circulation production. The factor of two difference in their resolution verifies that the shear layer is sufficiently resolved to capture the true value of circulation production.

[1] R. L. Bisplinghoff, H. Ashley, and R. L. Halfman, *Aeroelasticity*. Dover Corporation, 1996.

[2] J. D. Eldredge and A. R. Jones, "Leading-edge vortices: Mechanics and modeling," *Annual Review of Fluid Mechanics*, vol. 51, no. 1, pp. 75–104, 2019.

[3] D. J. Pines and F. Bohorquez, "Challenges facing future micro-air-vehicle development," *Journal of Aircraft*, vol. 43, no. 2, pp. 290–305, 2006.

[4] J. McMasters and M. Henderson, "Low-speed single-element airfoil synthesis," *Technical Soaring*, vol. 6, no. 2, pp. 1–21, 1980.

[5] P. Lissaman, "Low-Reynolds-number airfoils," *Annual Review of Fluid Mechanics*, vol. 15, no. 1, pp. 223–239, 1983.

[6] M. H. Dickinson and K. G. Gotz, "Unsteady aerodynamic performance of model wings at low Reynolds numbers," *Journal of Experimental Biology*, vol. 174, no. 1, pp. 45–64, 1993.

[7] D. Rival and C. Tropea, "Characteristics of pitching and plunging airfoils under dynamic-stall con-

ditions," *Journal of Aircraft*, vol. 47, no. 1, pp. 80–86, 2010.

[8] T. Yilmaz, M. Ol, and D. Rockwell, "Scaling of flow separation on a pitching low aspect ratio plate," *Journal of Fluids and Structures*, vol. 26, no. 6, pp. 1034–1041, 2010.

[9] K. O. Granlund, M. V. Ol, and L. P. Bernal, "Unsteady pitching flat plates," *Journal of Fluid Mechanics*, vol. 733, p. R5, 2013.

[10] J. D. Eldredge, "Numerical simulation of the fluid dynamics of 2d rigid body motion with the vortex particle method," *Journal of Computational Physics*, vol. 221, no. 2, pp. 626–648, 2007.

[11] M. Ol, J. Eldredge, and C. Wang, "High-amplitude pitch of a flat plate: an abstraction of perching and flapping," *International Journal of Micro Air Vehicles*, vol. 1, September 2009.

[12] M. R. Visbal, R. E. Gordnier, and M. C. Galbraith, "High-fidelity simulations of moving and flexible airfoils at low Reynolds numbers," *Experiments in*

Fluids, vol. 46, no. 5, pp. 903–922, 2009.

[13] D. J. Garmann and M. R. Visbal, "Numerical investigation of transitional flow over a rapidly pitching plate," *Physics of Fluids*, vol. 23, no. 9, 2011.

[14] A. Jones, C. Pitt Ford, and H. Babinsky, "Three-dimensional effects on sliding and waving wings," *Journal of Aircraft*, vol. 48, no. 2, pp. 633–644, 2011.

[15] S. K. Venkata and A. R. Jones, "Leading-edge vortex structure over multiple revolutions of a rotating wing," *Journal of Aircraft*, vol. 50, no. 4, pp. 1312–1316, 2013.

[16] F. Manar, A. Medina, and A. R. Jones, "Tip vortex structure and aerodynamic loading on rotating wings in confined spaces," *Experiments in Fluids*, vol. 55, no. 9, pp. 1–18, 2014.

[17] M. Bross and D. Rockwell, "Flow structure on a simultaneously pitching and rotating wing," *Journal of Fluid Mechanics*, vol. 756, pp. 354–383, 2014.

[18] Z. R. Carr, A. C. DeVoria, and M. J. Ringuette, "Aspect-ratio effects on rotating wings: circulation and forces," *Journal of Fluid Mechanics*, vol. 767, pp. 497–525, 2015.

[19] D. J. Garmann, M. R. Visbal, and P. D. Orkwis, "Three-dimensional flow structure and aerodynamic loading on a revolving wing," *Physics of Fluids*, vol. 25, no. 3, p. 034101, 2013.

[20] P. Hammer, A. Altman, and F. Eastep, "Validation of a discrete vortex method for low Reynolds number unsteady flows," *AIAA Journal*, 2014.

[21] C. Wang and J. D. Eldredge, "Low-order phenomenological modeling of leading-edge vortex formation," *Theoretical and Computational Fluid Dynamics*, vol. 27, no. 5, pp. 577–598, 2013.

[22] G. J. Leishman, *Principles of Helicopter Aerodynamics*. Cambridge University Press, 2006.

[23] C. Ellington, "The aerodynamics of hovering insect flight. V. a vortex theory," *Philosophical Transactions of the Royal Society B: Biological Sciences*, vol. 305, no. 1122, pp. 115–144, 1984.

[24] C. Pitt Ford and H. Babinsky, "Lift and the leading-edge vortex," *Journal of Fluid Mechanics*, vol. 720, pp. 280–313, 2013.

[25] C. J. Wojcik and J. H. Buchholz, "Vorticity transport in the leading-edge vortex on a rotating blade," *Journal of Fluid Mechanics*, vol. 743, pp. 249–261, 2014.

[26] J. H. Buchholz, M. A. Green, and A. J. Smits, "Scaling the circulation shed by a pitching panel," *Journal of Fluid Mechanics*, vol. 688, pp. 591–601, 2011.

[27] P. Sattari, D. E. Rival, R. J. Martinuzzi, and C. Tropea, "Growth and separation of a start-up vortex from a two-dimensional shear layer," *Physics of Fluids*, vol. 24, no. 10, p. 107102, 2012.

[28] J. Kriegseis, M. Kinzel, and D. E. Rival, "On the persistence of memory: Do initial conditions impact vortex formation?," *Journal of Fluid Mechanics*, vol. 736, pp. 91–106, 2013.

[29] J. G. Wong, J. Kriegseis, and D. E. Rival, "An investigation into vortex growth and stabilization for

[30] A. Widmann and C. Tropea, "Parameters influencing vortex growth and detachment on unsteady aerodynamic profiles," *Journal of Fluid Mechanics*, vol. 773, pp. 432–459, 2015.

[31] A. E. Panah, J. M. Akkala, and J. H. Buchholz, "Vorticity transport and the leading-edge vortex of a plunging airfoil," *Experiments in Fluids*, vol. 56, no. 8, pp. 1–15, 2015.

[32] M. Lighthill, *Laminar Boundary Layers*. Oxford University Press, 1963.

[33] H. Wagner, "Über die Entstehung des dynamischen Auftriebes von Tragflügeln," *ZAMM-Journal of Applied Mathematics and Mechanics/Zeitschrift für Angewandte Mathematik und Mechanik*, vol. 5, no. 1, pp. 17–35, 1925.

[34] H. Glauert, *The force and moment on an oscillating aerofoil*. HM Stationery Office, 1929.

[35] T. Theodorsen, "General theory of aerodynamic instability and the mechanism of flutter," *NACA Report*, no. 496, 1935.

[36] D. Pullin and Z. J. Wang, "Unsteady forces on an accelerating plate and application to hovering insect flight," *Journal of Fluid Mechanics*, vol. 509, pp. 1–21, 2004.

[37] M. N. J. Moore, "Torsional spring is the optimal flexibility arrangement for thrust production of a flapping wing," *Physics of Fluids*, vol. 27, no. 9, 2015.

[38] E. C. Polhamus, "Predictions of vortex-lift characteristics by a leading-edge suction analogy," *Journal of aircraft*, vol. 8, no. 4, pp. 193–199, 1971.

[39] Y. S. Baik, L. P. Bernal, K. Granlund, and M. V. Ol, "Unsteady force generation and vortex dynamics of pitching and plunging aerofoils," *Journal of Fluid Mechanics*, vol. 709, pp. 37–68, 2012.

[40] M. A. Jones, "The separated flow of an inviscid fluid around a moving flat plate," *Journal of Fluid Mechanics*, vol. 496, pp. 405–441, 2003.

[41] S. Ansari, R. Żbikowski, and K. Knowles, "Nonlinear unsteady aerodynamic model for insect-like flapping wings in the hover. Part 1: Methodology and analysis," *Proceedings of the Institution of Mechanical Engineers, Part G: Journal of Aerospace Engineering*, vol. 220, no. 2, pp. 61–83, 2006.

[42] J. Katz, "A discrete vortex method for the nonsteady separated flow over an airfoil," *Journal of Fluid Mechanics*, vol. 102, pp. 315–328, 1981.

[43] R. K. Shukla and J. D. Eldredge, "An inviscid model for vortex shedding from a deforming body," *Theoretical and Computational Fluid Dynamics*, vol. 21, no. 5, pp. 343–368, 2007.

[44] K. Ramesh, A. Gopalarathnam, J. R. Edwards, M. V. Ol, and K. Granlund, "An unsteady airfoil theory applied to pitching motions validated against experiment and computation," *Theoretical and Computational Fluid Dynamics*, vol. 27, no. 6, pp. 843–864, 2013.

[45] S. P. Sane and M. H. Dickinson, "The aerodynamic

effects of wing rotation and a revised quasi-steady model of flapping flight," *Journal of Experimental Biology*, vol. 205, no. 8, pp. 1087–1096, 2002.

[46] H. E. Taha, M. R. Hajj, and P. S. Beran, "State-space representation of the unsteady aerodynamics of flapping flight," *Aerospace Science and Technology*, vol. 34, pp. 1–11, 2014.

[47] H. Babinsky, P. Stevens, A. R. Jones, L. P. Bernal, and M. V. Ol, "Low order modeling of lift forces for unsteady pitching and surging wings," in *54th AIAA Aerospace Sciences Meeting*, 2016.

[48] F. M. Bos, D. Lentink, B. Van Oudheusden, and H. Bijl, "Influence of wing kinematics on aerodynamic performance in hovering insect flight," *Journal of Fluid Mechanics*, vol. 594, pp. 341–368, 2008.

[49] P. Trizila, C.-K. Kang, H. Aono, W. Shyy, and M. Visbal, "Low-Reynolds-number aerodynamics of a flapping rigid flat plate," *AIAA Journal*, vol. 49, no. 4, pp. 806–823, 2011.

[50] J. Lankford, D. Mayo, and I. Chopra, "Computational investigation of insect-based flapping wings for micro air vehicle applications," *International Journal of Micro Air Vehicles*, 2016.

[51] J. D. Anderson Jr, *Fundamentals of Aerodynamics*. McGraw-Hill Education, 2010.

[52] J. Katz and A. Plotkin, *Low-speed aerodynamics*. Cambridge University Press, 2nd ed., 2001.

[53] R. L. Panton, *Incompressible Flow*. John Wiley & Sons, 3rd ed., 2006.

[54] L. M. Milne-Thomson, *Theoretical Hydrodynamics*. Dover Publications, fifth ed., 1968.

[55] G. K. Batchelor, *An Introduction to Fluid Dynamics*. Cambridge University Press, 1967.

[56] X. Xia and K. Mohseni, "Lift evaluation of a two-dimensional pitching flat plate," *Physics of Fluids*, vol. 25, no. 9, p. 091901, 2013.

[57] S. Ansari, R. Żbikowski, and K. Knowles, "Non-linear unsteady aerodynamic model for insect-like flapping wings in the hover. Part 2: Implementation and validation," *Proceedings of the Institution of Mechanical Engineers, Part G: Journal of Aerospace Engineering*, vol. 220, no. 3, pp. 169–186, 2006.

[58] F. Minotti, "Unsteady two-dimensional theory of a flapping wing," *Physical Review E*, vol. 66, no. 5, 2002.

[59] H. Glauert, *The Elements of Aerofoil and Airscrew Theory*. Cambridge University Press, 2nd ed., 1947.

[60] M. A. Jones and M. J. Shelley, "Falling cards," *Journal of Fluid Mechanics*, vol. 540, pp. 393–425, 2005.

[61] J. L. Hess and A. Smith, "Calculation of non-lifting potential flow about arbitrary three-dimensional bodies," tech. rep., Douglas Aircraft Co Long Beach CA, 1962.

[62] J. Hess, "Panel methods in computational fluid dynamics," *Annual Review of Fluid Mechanics*, vol. 22, no. 1, pp. 255–274, 1990.

[63] G.-H. Cottet and P. D. Koumoutsakos, *Vortex Methods: Theory and Practice*. Cambridge University Press, 2000.

[64] P. G. Saffman, *Vortex Dynamics*. Cambridge University Press, 1992.

[65] A. J. Chorin, "Numerical study of slightly viscous flow," *Journal of Fluid Mechanics*, vol. 57, no. 4, pp. 785–796, 1973.

[66] A. J. Chorin and P. S. Bernard, "Discretization of a vortex sheet, with an example of roll-up," *Journal of Computational Physics*, vol. 13, no. 3, pp. 423–429, 1973.

[67] R. Krasny, "Desingularization of periodic vortex sheet roll-up," *Journal of Computational Physics*, vol. 65, no. 2, pp. 292–313, 1986.

[68] G. H. Vatistas, V. Kozel, and W. Mih, "A simpler model for concentrated vortices," *Experiments in Fluids*, vol. 11, no. 1, pp. 73–76, 1991.

[69] N. J. Zabusky, M. Hughes, and K. Roberts, "Contour dynamics for the Euler equations in two dimensions," *Journal of Computational Physics*, vol. 30, no. 1, pp. 96–106, 1979.

[70] M. J. Stock, W. J. Dahm, and G. Tryggvason, "Impact of a vortex ring on a density interface using a regularized inviscid vortex sheet method," *Journal of Computational Physics*, vol. 227, no. 21, pp. 9021–9043, 2008.

[71] B. A. Roccia, S. Preidikman, J. C. Massa, and D. T. Mook, "Modified unsteady vortex-lattice method to study flapping wings in hover flight," *AIAA Journal*, vol. 51, no. 11, pp. 2628–2642, 2013.

[72] M. Stock, "Summary of vortex method literature." via http://markjstock.org/research/, downloaded 12/24/2017, 2006.

[73] G. Winckelmans and A. Leonard, "Contributions to vortex particle methods for the computation of three-dimensional incompressible unsteady flows," *Journal of Computational Physics*, vol. 109, no. 2, pp. 247–273, 1993.

[74] S. Shankar and L. Van Dommelen, "A new diffusion procedure for vortex methods," *Journal of Computational Physics*, vol. 127, no. 1, pp. 88–109, 1996.

[75] M. Kirchhart and S. Obi, "A splitting-free vorticity redistribution method," *Journal of Computational Physics*, vol. 330, pp. 282–295, 2017.

[76] M. Drela, "XFOIL: An analysis and design system for low Reynolds number airfoils," in *Low Reynolds number aerodynamics*, pp. 1–12, Springer, 1989.

[77] T. Sarpkaya, "Computational methods with vortices," *ASME, Transactions, Journal of Fluids Engineering*, vol. 111, pp. 5–52, 1989.

[78] R. Krasny, "Vortex sheet computations: roll-up, wakes, separation," *Lectures in Applied Mathematics*, vol. 28, no. 1, pp. 385–401, 1991.

[79] R. Krasny and M. Nitsche, "The onset of chaos in vortex sheet flow," *Journal of Fluid Mechanics*, vol. 454, pp. 47–69, 2002.

[80] X. Xia and K. Mohseni, "Unsteady aerodynamics and vortex-sheet formation of a two-dimensional airfoil," *Journal of Fluid Mechanics*, vol. 830, pp. 439–478, 2017.

[81] J. G. Leishman and T. Beddoes, "A semi-empirical model for dynamic stall," *Journal of the American Helicopter society*, vol. 34, no. 3, pp. 3–17, 1989.

[82] J. O. Dabiri, "Optimal vortex formation as a unifying principle in biological propulsion," *Annual review of fluid mechanics*, vol. 41, pp. 17–33, 2009.

[83] I. H. Abbott and A. E. Von Doenhoff, *Theory of Wing Sections, Including a Summary of Airfoil Data.* Courier Corporation, 1959.

[84] C. Brennen, "A review of added mass and fluid inertial forces.," tech. rep., Naval Civil Engineering Laboratory, 1982.

[85] G. J. Berman and Z. J. Wang, "Energy-minimizing kinematics in hovering insect flight," *Journal of Fluid Mechanics*, vol. 582, pp. 153–168, 2007.

[86] F. Manar, P. Mancini, D. Mayo, and A. R. Jones, "Comparison of rotating and translating wings: force production and vortex characteristics," *AIAA Journal*, 2016.

[87] T. VonKarman and W. Sears, "Airfoil theory for non-uniform motion," *Journal of the Aeronautical Sciences*, vol. 5, no. 10, pp. 379–390, 1938.

[88] J. M. Greenberg, "Airfoil in sinusoidal motion in a pulsating stream," Tech. Rep. 1326, NACA, June 1947.

[89] J. Leishman and K. Nguyen, "State-space representation of unsteady airfoil behavior.," *AIAA Journal*, vol. 28, no. 5, pp. 836–844, 1990.

[90] H. G. Küssner, "Stresses produced in airplane wings by gusts," *NACA-TM-654*, 1932.

[91] W. R. Sears, "Some aspects of non-stationary airfoil theory and its practical application," *Journal of the Aeronautical Sciences*, vol. 8, no. 3, 1941.

[92] J. Leishman, "Validation of approximate indicial aerodynamic functions for two-dimensional subsonic flow," *Journal of Aircraft*, vol. 25, no. 10, pp. 914–922, 1988.

[93] K. C. Hall and S. R. Hall, "Minimum induced power requirements for flapping flight," *Journal of Fluid Mechanics*, vol. 323, pp. 285–315, 1996.

[94] K. C. Hall, S. A. Pigott, and S. R. Hall, "Power requirements for large-amplitude flapping flight," *Journal of Aircraft*, vol. 35, no. 3, pp. 352–361, 1998.

[95] H. Salehipour and D. J. Willis, "A coupled kinematics–energetics model for predicting energy efficient flapping flight," *Journal of Theoretical Biology*, vol. 318, pp. 173–196, 2013.

[96] D. Pullin, "The large-scale structure of unsteady self-similar rolled-up vortex sheets," *Journal of Fluid Mechanics*, vol. 88, no. 3, pp. 401–430, 1978.

[97] L. Cortelezzi and A. Leonard, "Point vortex model of the unsteady separated flow past a semi-infinite plate with transverse motion," *Fluid Dynamics Research*, vol. 11, no. 6, p. 263, 1993.

[98] C. Brown and W. Michael, "Effect of leading-edge separation on the lift of a delta wing," *Journal of the Aeronautical Sciences*, vol. 21, no. 10, 1954.

[99] D. Darakananda, J. Eldredge, T. Colonius, and D. R. Williams, "A vortex sheet/point vortex dynamical model for unsteady separated flows," in *54th AIAA Aerospace Sciences Meeting*, pp. 4–8, 2016.

[100] L. Greengard, "The FMMLIB2D suite." https://cims.nyu.edu/cmcl/fmm2dlib/fmm2dlib.html.

[101] J. Wu, "Theory for aerodynamic force and moment in viscous flows," *AIAA Journal*, vol. 19, no. 4, pp. 432–441, 1981.

[102] C. Chabalko, R. D. Snyder, P. S. Beran, and G. Parker, "The physics of an optimized flapping wing micro air vehicle," in *47th AIAA Aerospace Sciences Meeting*, pp. 2009–801, 2009.

[103] F. Manar and A. R. Jones, "Transient response of a single degree-of-freedom wing at high angle-of-attack," *AIAA Journal*, pp. 1–12, 2017.

[104] L. Graftieaux, M. Michard, and N. Grosjean, "Combining PIV, POD and vortex identification algorithms for the study of unsteady turbulent swirling flows," *Measurement Science and Technology*, vol. 12, no. 9, p. 1422, 2001.